CRYSTAL GROWTH & DESIGN

Review

Cite This: *Cryst. Growth Des.* 2019, 19, 7439−7462

pubs.acs.org/crystal

Synthesis and Applications of Isoreticular Metal−Organic Frameworks IRMOFs-*n* (*n* = 1, 3, 6, 8)

Zehan Mai and Dingxin Liu*

State Key Laboratory of Optoelectronic Materials and Technologies, Nanotechnology Research Center, School of Materials Science & Engineering, Sun Yat-sen University, Guangzhou, 510275 Guangdong, China

ABSTRACT: Isoreticular metal−organic frameworks (IRMOFs) are a series of MOFs that own similar network topology. By simple substitution of organic linkers of IRMOF-1 (i.e., MOF-5), other IRMOFs can be obtained and have unique features such as large BET surface areas and high chemical stability. IRMOF has been exalted to be an important branch of MOFs because the unique features endow IRMOF with potential applications including adsorption, catalysis, and sensing. Large BET surface areas of IRMOFs make them candidates for adsorbing small gases such as H_2, CO_2, and CH_4. Additionally, IRMOF-3, IRMOF-6, and IRMOF-8 can separate various mixtures. Due to different catalytic active sites and pore sizes, IRMOFs can catalyze a wide range of reactions. For instance, IRMOF-1 is able to catalyze the Friedel−Crafts alkylation reaction because of its coordination-unsaturated open metal sites. NH_2-containing IRMOF-3 acts as a basic catalyst for Knoevenagel condensation. Many keen sensors have been fabricated based on luminescent IRMOF-1 and IRMOF-3. IRMOF-8 with high porosity can be utilized to synthesize electrochemical sensor. This Review mainly introduces the applications of IRMOFs-*n* (*n* = 1, 3, 6, 8) and their derivatives in adsorption, catalysis, and sensing. Moreover, different strategies for synthesis and modification of IRMOFs are compared and discussed in this Review. The experiments and proposed mechanisms related to the applications of IRMOFs-*n* (*n* = 1, 3, 6, 8) are also summarized to provide an overview of IRMOFs.

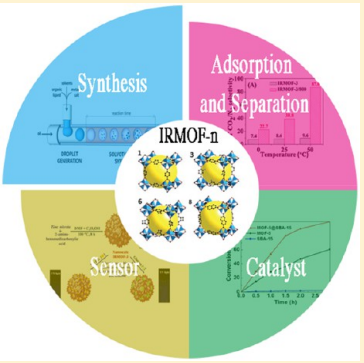

1. INTRODUCTION

1.1. IRMOFs. Metal−organic framework (MOF) is the main class in the field of porous solid materials. This class of porous materials is synthesized by connecting metal nodes with various organic linkers.[1] Numerous kinds of MOFs have been synthesized successfully including zeolitic imidazolate framework (ZIF),[2,3] materials of Institut Lavoisier (MIL),[4−6] Hong-Kong University of Science and Technology (HKUST),[7−9] Northwest University (NU),[10−12] and so forth. MOFs have drawn the attention of many physicists and chemists because of their large pore volumes, high surface areas, and excellent tunability. These fascinating features endow MOFs with potential applications. For instance, MOFs have been employed as powerful adsorbents in different conditions,[13−15] efficient catalysts for some important reactions,[16−18] keen sensors,[19−21] and effective drug or biological substance carriers.[22−24]

IRMOF-1 (i.e., MOF-5) is one MOF that was first synthesized by the group of Omar M. Yaghi and has been well studied ever since its origin. By utilizing the strategy that included reticulating metal ions and organic carboxylate, the group of Omar M. Yaghi synthesized a class of porous materials which were named isoreticular MOFs (IRMOFs).[25] The series of IRMOFs shares the similar **pcu** topology of IRMOF-1 as shown in Figure 1. One can construct IRMOFs from octahedral Zn−O−C clusters and varied organic linkers. Therefore, the physical and chemical properties of IRMOFs are quite different. As demonstrated in Table 1, the surface areas and pore volumes of different IRMOFs vary with their organic linkers. We also compared these characters of IRMOFs with other MOFs that have **pcu** or other topologies in Table 1.

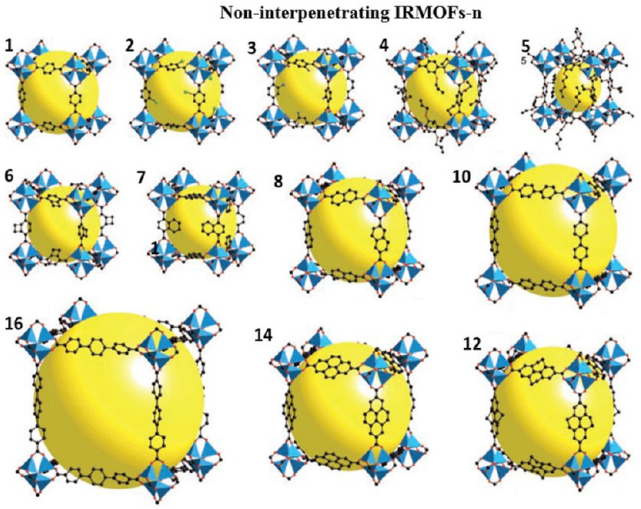

Figure 1. Illustration of IRMOFs-*n* (*n* = 1−8, 10, 12, 14, 16) that are non-interpenetrating IRMOFs. (Reproduced with permission from ref 139. Copyright Elsevier, 2018.)

IRMOF-1 is still the frontier domain of MOF research and it is the prototype of all IRMOFs. The linkers of IRMOF-3 and

Received: July 5, 2019
Published: October 23, 2019

DOI: 10.1021/acs.cgd.9b00879
Cryst. Growth Des. 2019, 19, 7439−7462

Table 1. Comparison of Metal Nodes/Clusters, Ligands, Pore Volumes, and Surface Areas of IRMOFs-*n* with Other MOFs

MOF	metal nodes/clusters	ligands[a]	topology	pore volumes [$cm^3 \cdot g^{-1}$]	surface area[b] [$m^2 \cdot g^{-1}$]	ref
IRMOF-1	Zn_4O	BDC	**pcu**	1.22	2205 (BET surface area)	26
IRMOF-3	Zn_4O	2-NH_2-BDC	**pcu**	1.07	1568 (BET surface area)	26
IRMOF-6	Zn_4O	Cyclobutyl-BDC	**pcu**	1.14	2516 (BET surface area)	27,28
IRMOF-8	Zn_4O	2,6-NDC	**pcu**	0.39	1021 (BET surface area)	29
IRMOF-11	Zn_4O	HPDC	**pcu**	-	1911	30
IRMOF-18	Zn_4O	TMBDC	**pcu**	-	1501	30
NU-1100	$Zr_6O_4(OH)_4^{12+}$	L_4H	**ftw**	1.53	4020 (BET surface area)	31,32
MIL-100(Cr)	trimeric chromium(III) octahedral clusters	BTC	**mtn**	1.0	2700 (Langmuir surface area)	33,34
MIL-101(Cr)	trimeric chromium(III) octahedral clusters	BDC	**mtn**	1.9	5500 (Langmuir surface area)	33,34
ZIF-67	Co^{2+}	2-methylimidazole	**sod**	-	1319.9 (BET surface area) 1832.2 (Langmuir surface area)	35,36
ZIF-8	Zn^{2+}	MeIM	**sod**	-	1630 (BET surface area) 1810 (Langmuir surface area)	36,37
HKUST-1	Cu^{2+}	BTC	**tbo**	0.75	1568.5 (BET surface area) 2081.4 (Langmuir surface area)	7,38,39
$[Cu_6(L')_3(DMF)\cdot(H_2O)_5]_n\cdot(DMF)_x$	Cu^{2+}	H_4L'	**pcu**	0.72	2010 (BET surface area) 2665 (Langmuir surface area)	40
vanadium−salen based Cd-bpdc MOF	Cd^{2+}	$V^{IV}OL''$, bpdc	**pcu**	0.24	574 (BET surface area) 697 (Langmuir surface area)	41
JUC-135	Zn^{2+}	H_2DCPB	**pcu**	-	503.7 (BET surface area) 718.9 (Langmuir surface area)	42
JLU-MOF50	Zr_6 cluster	H_2MDCPB	**pcu**	-	1101 (BET surface area) 1404 (Langmuir surface area)	43

[a]BDC = benzene-1,4-dicarboxylate, NDC = naphthalenedicarboxylate, L_4H = 4-[2-[3,6,8-tris[2-(4-carboxyphenyl)-ethynyl]-pyren-1-yl]ethynyl]-benzoic acid, BTC = benzene-1,3,5-tricarboxylate, TMBDC = 2,3,5,6-tetramethylbenzene-1,4-dicarboxylic acid, HPDC = 4,5,9,10-Tetrahydro-2,7-pyrenedicarboxylic acid, MeIM = 2-methylimidazolate, H_4L' = 1,1-bis-[3,5-bis(carboxy) phenoxy]methane, L″ = (R,R)-(−)-1,2-cyclohexanediamino-N,N_0-bis(3-*tert*-butyl-5-(4-pyridyl)salicylidene), bdpc = biphenyl-4,4′-dicarboxylic acid, H_2DCPB = 1,3-di(4-carboxyphenyl)-benzene, H_2MDCPB = 1,3-di(4-carboxyphenyl) benzene. [b]Langmuir surface area from N_2 adsorption at 77 K; BET surface area from N_2 at 77 K.

IRMOF-6 are both the resultants of substitution reaction in the benzene ring of 1,4-benzenedicarboxylate (BDC). Among numerous IRMOFs, IRMOF-8 (non-interpenetrating) is a well-studied IRMOF with polycyclic aromatic hydrocarbon as linkers. Different linkers of IRMOFs-*n* (*n* = 1, 3, 6, 8) bring about their unique features and many applications relating to these features have been explored. Herein the applications of IRMOFs-*n* (*n* = 1, 3, 6, 8) and their derivatives in adsorption, catalysis, and sensing are introduced. In addition, diverse strategies for synthesis and modification of these IRMOFs are also summarized to give an overview.

1.2. Synthesis. The first and most commonly used solvothermal method of synthesizing IRMOFs is based on improved preparation of IRMOF-1 conducted by the group of Omar M. Yaghi in 2002. By employing *N*,*N*-diethylformamide (DEF) as solvent and dissolving $Zn(NO_3)_2\cdot 4H_2O$ and the acid form of 1,4-benzenedicarboxylate (BDC), the group obtained a mixture for reaction and heated it in the range of 85−105 °C in a closed container. In this way, crystalline IRMOF-1 was synthesized with high yield. Following the synthesis of IRMOF-1, other members of IRMOFs have been simply obtained by utilizing other organic linkers instead of BDC. Specifically, 2-NH_2-BDC and cyclobutyl-BDC are utilized in synthesizing IRMOF-3 and IRMOF-6, respectively. IRMOF-8 has been yielded through the replacement of BDC by 2,6-NDC.[25]

Though the solvothermal method is conventional and has been used by researchers up to now, the drawback of this method is apparent due to the long time needed for crystallization and forming a porous network. Hence, sonochemical synthesis of IRMOF-1 appears as an alternative method for the solvothermal method with the development of sonochemistry. The reagent of this synthesis is quite similar to those of the solvothermal method except the solvent. 1-Methyl-2-pyrrolidone (NMP) has been used as a substitute for DEF because NMP is more economical. By contrast, the researchers have obtained high quality IRMOF-1 crystal (S-MOF-5) eventually after sonication treatment that continued for 10 min. To examine the availability of the sonochemical method, S-MOF-5 has been compared with IRMOF-1 prepared via the previous convective heating method (C-MOF-5), and similar physicochemical properties between them have been found. The comparison is shown in Figure 2. Sonochemical synthesis also proves to be effective in lowering energy consumption.[44]

Generating and controlling defects is a synthetic strategy of MOFs that are designed for catalysis and sorption. Adjustment of the temperature as well as the amount of water and various

DOI: 10.1021/acs.cgd.9b00879
Cryst. Growth Des. 2019, 19, 7439−7462

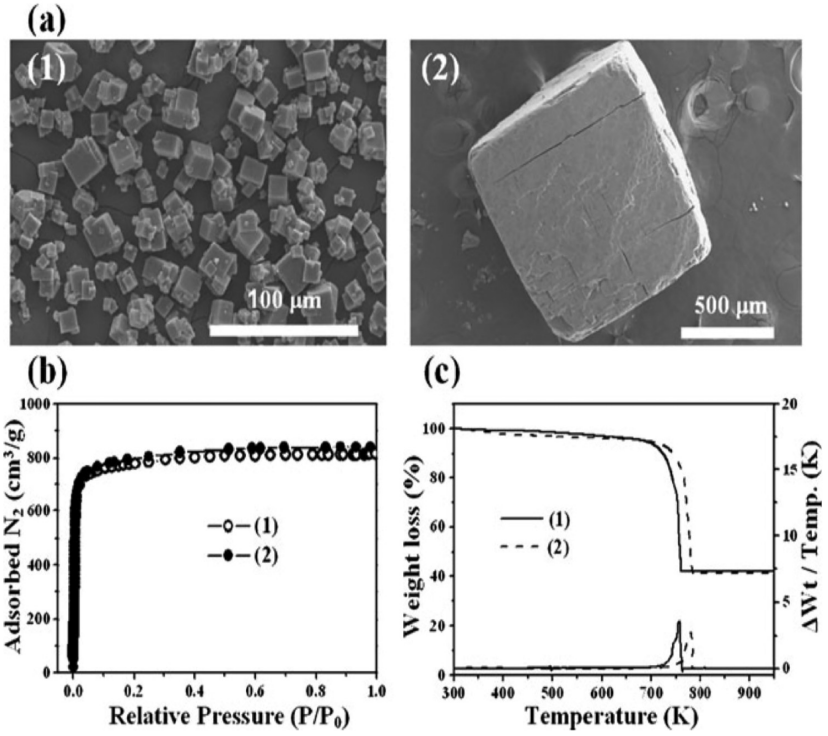

Figure 2. Physical and chemical properties of S-MOF-5 and C-MOF-5: (a) SEM images (1: S-MOF-5, 2: C-MOF-5), (b) adsorbed N_2 at the same temperature, (c) thermogravimetric analysis curves. (Reproduced with permission from ref 44. Copyright Royal Society of Chemistry, 2008.)

modulating acids in the reaction mixture can control the distribution of defects in MOFs. Defect engineering benefits the applications of MOFs in catalysis and sorption.[45,46] For instance, tuning the defects of UiO-66 leads to formation of active binding sites and makes the frameworks more open. Thus, it can enhance the absorbability of this MOF for actinide.[47] Synthesis of defective IRMOF-1 has been realized by utilizing 1,3,5-tris(4-carboxyphenyl)benzene (H_3BTB) during the synthesis. Park et al. utilized a solvothermal method and added a specific amount of H_3BTB to the reaction mixture. H_2BDC and H_3BTB act as linkers together and the morphologies of obtained IRMOF-1 varies with the amount of H_3BTB.[48] The types of defects in IRMOF-1 include partial removal of linkers and so forth. Molecular simulation has revealed that removal of linkers can influence the mechanical and chemical stability of IRMOF-1.[49] Therefore, synthesis of defective IRMOF-1 could be meaningful, and defect engineering is likely to open a new avenue for synthesizing other IRMOFs.

In the recent years, a more feasible and effective microfluidic strategy for synthesizing IRMOF-1 and IRMOF-3 has been put forward on the basis of the conventional solvothermal method. Precursor solution has been obtained by adding $Zn(NO_3)_2 \cdot 6H_2O$ and H_2BDC ($H_2BDC\text{-}NH_2$ for IRMOF-3) to *N,N*-dimethylformamide (DMF) and transformed into continuous phase and dispersed phase. Then, both phases have been injected into the microfluidic device and the droplet reactor has been streamed in a perfluoroalkoxyalkane (PFA) tube to synthesize products (Figure 3). What makes the microfluidic strategy appealing is that it is comprehensive, energy-efficient, and time-saving.[50]

Synthesizing MOFs at room temperature can save energy and push the industrial applications of MOF forward. Therefore, a novel method of synthesizing MOFs has been

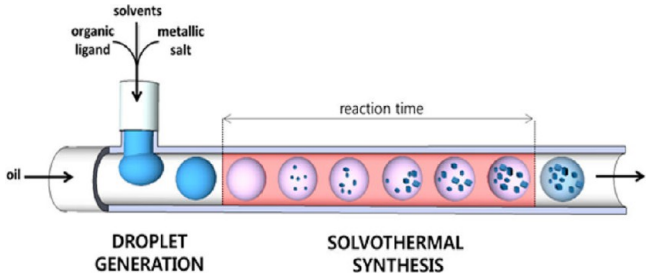

Figure 3. Graphical representation of the microfluidic strategy process. (Reproduced from ref 50.)

put forward by Zhao et al. in 2015 and utilized in the synthesis of IRMOF-3. In their research, hydroxy double salts (HDSs) have been used as the intermediates. The most important steps involved in the synthesis of IRMOF-3 are (1) reacting ZnO with $Zn(CH_3CO_2)_2 \cdot 2H_2O$ at room temperature to form (Zn, Zn) hydroxy acetate HDS and (2) reacting $H_2BDC\text{-}NH_2$ solution with HDS.[51] In addition to the above tactics, some novel methods such as the electrochemical method have been explored to synthesize IRMOFs without the limitation of special apparatus.[52]

2. APPLICATION OF IRMOFS

2.1. Adsorption and Separation. *2.1.1. IRMOF-1: Adsorption of Small Gases and Natural Gas.* Adsorption is one of the most significant applications of porous materials including MOFs. The use of MOF in adsorption is predicted to have a bright future in industrial equipment manufacture and environmental protection. The role of separation is important in both life and industry.[53]

There are many advantages of MOFs in adsorption and separation: (1) many MOFs are physically, thermally, and

DOI: 10.1021/acs.cgd.9b00879
Cryst. Growth Des. 2019, 19, 7439−7462

Table 2. Comparison of Gas Adsorption Properties of Some IRMOFs with other MOFs

material	N_2 uptake	H_2 adsorption capacity	CO_2 adsorption capacity	total CH_4 adsorption	ref
IRMOF-1	13.2 $mg·g^{-1}$ (77k, 1 atm)	13.2 $mg·g^{-1}$ (77k, 1 atm)	21.7 $mmol·g^{-1}$ (r.t., 35 bar)	241 $cm^3·g^{-1}$ (25 °C, 35 bar)	30,27,55
IRMOF-3	-	14.2 $mg·g^{-1}$ (77k, 1 atm)	18.7 $mmol·g^{-1}$ (r.t., 35 bar)	228 $cm^3·g^{-1}$ (25 °C,36.5 bar)	27,28,55
IRMOF-6	-	14.8 $mg·g^{-1}$ (77k, 1 atm)	19.5 $mmol·g^{-1}$ (r.t., 35 bar)	272 $cm^3·g^{-1}$ (25 °C, 36.5 bar)	27,28,55
IRMOF-8	421 $mg·g^{-1}$ (77k, 1 atm)	15.0 $mg·g^{-1}$ (77k, 1 atm)	-	254 $cm^3·g^{-1}$ (25 °C, 35 bar)	30,56
IRMOF-11	548 $mg·g^{-1}$ (77k, 1 atm)	16.2 $mg·g^{-1}$ (77k, 1 atm)	14.7 $mmol·g^{-1}$ (r.t., 35 bar)	-	30,27
IRMOF-18	431 $mg·g^{-1}$ (77k, 1 atm)	8.9 $mg·g^{-1}$ (77k, 1 atm)	-	-	30
$[Cu_6(L')_3(DMF)·(H_2O)_5]_n·(DMF)_x$	633 $cm^3·g^{-1}$ (77K, 1 bar)	-	91 $cm^3·g^{-1}$ (273 K, 5999 mmHg)	90 $cm^3·g^{-1}$ (295 K, 6026 mmHg)	40
vanadium−salen based Cd-bpdc MOF	-	10.55 $mg·g^{-1}$ (77k, 1 bar)	51 $cm^3·g^{-1}$ (273 K, 1 bar)	-	41
MIL-100(Cr)	-	-	18 $mmol·g^{-1}$ (304 K, 5.0 MPa)	9.5 $mmol·g^{-1}$ (303 K, 60 atm)	57,58
MIL-101(Cr)	-	-	40 $mmol·g^{-1}$ (304 K, 5.0 MPa)	13.6 $mmol·g^{-1}$ (303 K, 60 atm)	57,58
ZIF-67	-	15.3 $mg·g^{-1}$ (77k, 1 bar)	21.1 $cm^3·g^{-1}$ (298 K, 1 bar)	-	59,60
ZIF-8	0.08 $mmol·g^{-1}$ (25 °C, 1 bar)	14.3 $mg·g^{-1}$ (77k, 1 bar)	0.66 $mmol·g^{-1}$ (25 °C, 1 bar)	0.28 $mmol·g^{-1}$ (25 °C, 1 bar)	59,61
HKUST-1	-	22.7 $mg·g^{-1}$ (77k, 1 bar)	7.92 $mmol·g^{-1}$ (196 K, 1 bar)	68 $cm^3·cm^{-3}$ (25 °C, 5.8 bar)	62−64

chemically stable enough to be utilized as adsorbents in some tough environments; (2) MOFs possess high surface areas and pore volumes which are beneficial for the capture and storage of adsorbate; (3) the excellent tunability of MOF makes it possible to enhance the adsorption performance of them through modification.

As a class of MOF, IRMOFs have the potential to be outstanding adsorbents. By variation of organic linkers, IRMOFs achieve the goal of expanding the pore size with the topology maintained. This facile design makes IRMOFs meet the criteria of adsorption of adsorbent molecules in different sizes. The functional groups of the organic linkers of IRMOFs can affect MOFs' attraction for different kinds of molecules, which also enhances the separation ability of IRMOFs. Studying adsorption of small gaseous molecules can not only provide a vital method to evaluate the adsorption ability of IRMOFs but also inspire us to utilize them in protecting the environment and storing fuel gases (such as H_2 and CH_4). The data of adsorption of several small gases (N_2, H_2, CO_2, and CH_4) by IRMOFs and other MOFs is listed in Table 2. IRMOF-1 is considered a milestone of MOF research. It is one of the most highly porous MOFs and it has open 3D pores that are of ∼11.5 Å. However, the demerit of IRMOF-1 is that it is not stable enough in moist conditions.[54] This demerit is likely to limit the early mainstream of research to adsorption in the gaseous phase (Table 3).

Hydrogen (H_2) and methane (CH_4) are two clean energy resources that have high practical value, while the expansion of their applications relies on the improvement of the storage technique. The storage of these fuel gases must be attainable under practical pressure and temperature conditions.[25] As shown in Table 2, the methane adsorption capacity of IRMOF-1 (241 $cm^3·g^{-1}$ at 25 °C, 35 bar) is higher than that of IRMOF-3 (228 $cm^3·g^{-1}$ at 25 °C, 36.5 bar) even at lower pressure. It is considered that the isolated linkers provide a platform for IRMOF-1 to sorb molecules from all sides, which helps to improve the adsorption of gases (including hydrogen),[68] while the hydrogen adsorption capacity of pure IRMOF-1 (13.2 $mg·g^{-1}$ at 77k, 1 atm) is not as ideal as predicted. The metal nodes/cluster and the organic linkers of MOF are two potential sites for adsorption of gas molecules. H_2 proves to adsorb on both sites. As for methane and nitrogen, the organic linker of IRMOF plays a key role in the adsorption of both of them according to the investigation by Raman spectroscopy.[72] As a result, the unsatisfactory performance of IRMOF-1 in sorption of methane can be improved by substitution of its organic linker. For example, IRMOF-6 is a better sorbent of methane than IRMOF-1.

Table 3. Some Applications of IRMOFs-*n* (*n* = 1, 3, 6, 8) and Their Derivatives in Adsorption and Separation

IRMOF	applications in adsorption and separation (materials)	ref
IRMOF-1	(1) adsorption of gaseous contaminants especially for ammonia (pristine IRMOF-1) (2) storage of natural gas, i.e., NG (pristine IRMOF-1) (3) storage of H_2 (modified IRMOF-1 via spillover)	26,29,65
IRMOF-3	(1) adsorption of gaseous contaminants especially for ammonia and chlorine (pristine IRMOF-3) (2) selective adsorption of CO_2 from N_2 (pristine IRMOF-3, enhanced in NCMs from carbonization of IRMOF-3) (3) capturing dibenzothiophene, i.e., DBT (IRMOF-3-Ag-*n*)	26,66
IRMOF-6	(1) huge storage of methane (pristine IRMOF-6) (2) storage of H_2 (pristine IRMOF-6) (2) separation of C_4−C_6 alkene isomer mixture. (pristine IRMOF-6)	25,67−69
IRMOF-8	(1) storage of H_2 (pristine IRMOF-8, enhanced in modified IRMOF-8 via spillover) (2) elective adsorption of ethane from ethylene (pristine IRMOF-8)	29,68,70,71

DOI: 10.1021/acs.cgd.9b00879
Cryst. Growth Des. 2019, 19, 7439−7462

Excess carbon dioxide (CO_2) and other greenhouse gases is a cause of the greenhouse effect. Effective and efficient carbon capture (CC) is sure to alleviate the greenhouse effect. MOF is appealing in the application of adsorbing CO_2.[73] From Table 2, one can find clearly that the CO_2 sorption capacity of IRMOF-1 (21.7 mmol·g^{-1} at room temperature, 35 bar) is the greatest among IRMOFs-*n* (*n* = 3, 6, 8, 11, 18). Therefore, pure IRMOF-1 is identified as an outstanding adsorbent of CO_2. Moreover, the advantage of IRMOFs in adsorption of CO_2 is proven by comparison with MOF-2, Norit RB2, MOF-505, and MOF-74, but not MOF-177 (Figure 4).[27]

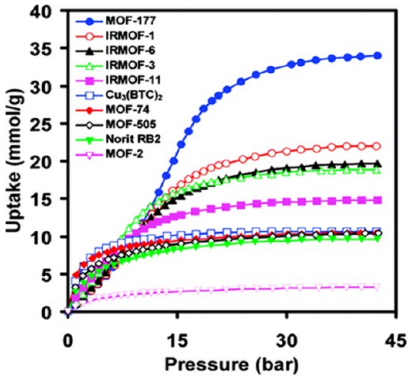

Figure 4. CO_2 capacities for IRMOFs-*n* (*n* = 1, 3, 6) and other MOFs at ambient temperature. (Reproduced from ref 27.)

Activated carbon is a widely used porous material for sorption. One of the practical applications of activated carbon is air purification. Nowadays, MOFs are also regarded as alternatives for activated carbon in this field. In the dynamic adsorption experiments, it has been found that the ammonia adsorption capacity of IRMOF-1 is 6-fold of undoped activated carbon.[26] Though the capacities of other harmful gases (chlorine and for forth) are not as high as that of its analog IRMOF-3, IRMOF-1 still shows potential as a manufacturing air purifier.

Natural gas (NG) is an energy resource with wide applications because it is economical, clean, and easy to obtain. The tunable nature of MOFs attracts more attention for utilizing them in storage of NG. Evaluation of the NG storage performance of material cannot only rely on the methane capacity, because the effect of higher hydrocarbon such as ethane (3.3%) and propane (0.7%) mixed in the NG should also be taken into account. That is why Zhang et al. have come up with a thermodynamic tank model.[74] The tools they have used are molecular simulations and macroscopic thermodynamics. According to their model, IRMOF-1 proves to be an eligible candidate that has better performance than NU-111 but not as good as IRMOF-14 and IRMOF-20. More significantly, they have discovered four general conditions of ideal MOF candidates for storage of NG: 0.9, 1850 m^2·cm^{-3}, 5500 m^2·g^{-1}, 10 kJ·mol^{-1}, respectively, for helium void fraction, volumetric surface area, gravimetric surface area, and heat of sorption of CH_4 when the loading is low. These conditions also inspire evaluation of the NG storage performance of IRMOF-3, IRMOF-6, and IRMOF-8.

To our knowledge, some methods have been put forward in order to enhance the hydrogen storage of IRMOF-1. As mentioned above, the adsorption of hydrogen is related to both the metal oxide clusters and the organic components of IRMOF-1, which is confirmed by previous inelastic neutron scattering studies.[68] The use of spillover for H_2 storage is representative of the physical method to make IRMOF-1 a more efficient adsorbent. This method has been first used in carbon materials to increase their storage capacities, and it needs utilization of catalysts that are able to dissociate H_2. Concretely speaking, the method has been operated by physically mixing a secondary spillover receptor (namely MOF) and catalyst (active carbon which is support of 5 wt % Pt). IRMOF-1 and IRMOF-8 have been selected to undergo this handling, and then, the products have been tested for their hydrogen capacities at room temperature over a range of pressure. The results show that the hydrogen storage performances of both IRMOFs are improved. For instance, the enhancement factor is 3.3 for IRMOF-1 at 10 MPa.[29] Though such handling has brought significant enhancement, there is still room for improvement because creating physical "bridges" between IRMOF and catalyst might increase the contacts to accelerate secondary spillover. Based on this hypothesis, Li and Yang have created carbon bridges with utilization of sucrose as the precursor.[70] The product manufactured in this way exhibits an enhancement factor of 2 in comparison to the previous physical mixture of IRMOF and catalyst. The hydrogen storage by spillover is an effective technique and can be transplanted for the application of other materials (such as IRMOF-9, IRMOF-993, COF-1, and COF-5), which has been confirmed by existing experiments.[75] Therefore, this technique may be utilized for enhancing the hydrogen capacities of other IRMOFs besides IRMOF-1 and IRMOF-8.

As for the applications of IRMOF-1 in the field of adsorption and separation in aqueous solution, the unavoidable problem dealt with by researchers is the hydrostability of IRMOF-1. IRMOF-1 is less stable in the presence of water than HKUST-1 and far less stable than MIL-100.[54] The lack of hydrostability limits the practical applications of IRMOF-1 such as removing contaminants from aquatic environments. With an aim to overcome this drawback, researchers have come up with some solutions. These include the following: (1) innovation in the synthesis of IRMOF-1 such as the microfluidic strategy process that is introduced above,[50] (2) limiting the growth of IRMOF-1 within the pores of a porous material like mesoporous silica and so on,[76] (3) hybridizing IRMOF-1 with other materials that have outstanding hydrostability such as attapulgite.[77]

2.1.2. IRMOF-3: Adsorption of Small Gases, Sulfur Compounds, and Selective CO_2/N_2 Adsorption. Though the structure of IRMOF-3 is no more different than that of amino-functionalized IRMOF-1, this unique functional group brings a different nature to IRMOF-3 and makes it possible to synthesize ideal materials for wider applications by further modification of it. Ammonia is one of most common gaseous contaminants in the environment, and there are always hydrogen bonds formed among the molecules. As we mentioned above, IRMOF-1 has the potential to be used for removing ammonia. Benefiting from the amine group, the adsorption capacity of IRMOF-3 for ammonia is 105 times as large as that of BPL carbon, and it is also an improvement over IRMOF-1. Moreover, the performance of IRMOF-3 in adsorbing chlorine is eminent as expected. These results have been attributed to the strong interaction between adsorbate molecules and amine groups of IRMOF-3.[26]

DOI: 10.1021/acs.cgd.9b00879
Cryst. Growth Des. 2019, 19, 7439−7462

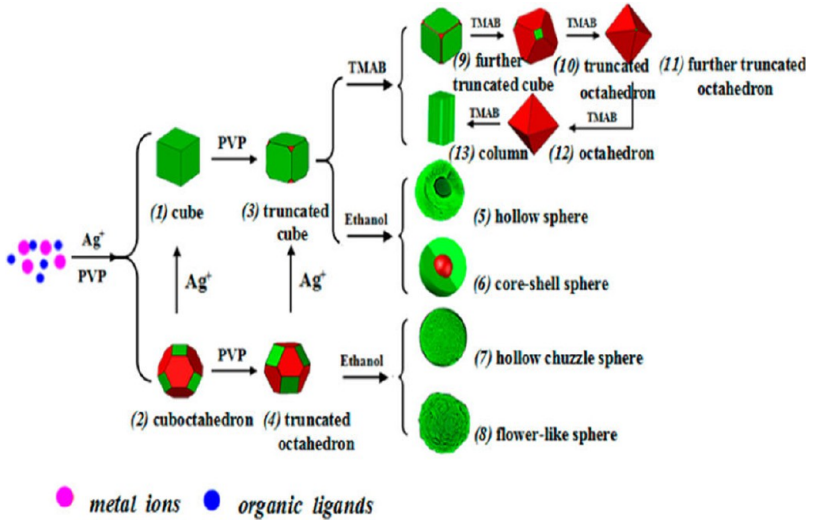

Figure 5. Illustration of the process of synthesizing IRMOF-3-Ag-*n* with various morphologies. (Reproduced from ref 69.)

Air-quality problems are among the concerns in environmental protection. Providing fuels without or with only a few sulfur compounds is an effective way to reduce the harm caused by vehicle exhaust. Therefore, the synthesis of materials that are able to adsorb sulfur compounds (such as thiophenic compounds) is significant. Based on the precedent that MOFs can be outstanding adsorbents, utilizing IRMOF-3 as an adsorbent of sulfur compounds is a feasible scheme. However, the performance of pristine IRMOF-3 is not comparable to practical needs. Due to this, IRMOF-3-Ag-*n* have been synthesized and eventually proven to capture dibenzothiophene (DBT) with larger capacities than their original framework.[69] Poly(vinylpyrrolidone), $AgNO_3$, TMAB, and solvent (DMF−ethanol) play various roles in the one-pot synthesis of IRMOF-3-Ag-*n*. For instance, PVP can change the interfacial free energy to control the growth of crystals with the help of $AgNO_3$. The kinetics of reaction is connected with TMAB for its role as a charge balancing template. Because of the effect of different modulators, IRMOF-3-Ag-*n* with various morphologies have been synthesized (Figure 5). The surface areas of IRMOF-3-Ag-*n* are lower than that of IRMOF-3. However, several kinds of IRMOF-3-Ag-*n* (such as $n = 1-5, 7$) have been tested to enhance the performance of IRMOF-3 in removing DBT especially for IRMOF-3-Ag-5, whose morphology is a hollow sphere structure. The enhanced property might be the result of π-complexation between dibenzothiophene and Ag nanoparticles.[69]

Different from conventional modifications of MOFs (like Atomic Layer Deposition and so on), direct carbonization of IRMOF-3 is a new, effective method that indicates the rosy prospect of IRMOF-3 in gas adsorption. The resultant of direct carbonization of IRMOF-3 is an N-doped carbon monolith (NCM) (Figure 6a). As is known to us, some materials can gain a more marvelous ability of sorption after nitrogen doping. Such practices in MOFs and their derived materials have also proven to be feasible.[78−80] 2-Aminobenzene-1,4-dicarboxylic acid that IRMOF-3 includes can act as the nitrogen source of doping, so carbonizing IRMOF-3 can synthesize new, more attractive materials. Another advantage of carbonizing IRMOF-3 to synthesize new materials is that the unique ZnO clusters play key roles in transforming the microporous structure of IRMOF-3 to a meso−macroporous one. Experiments have

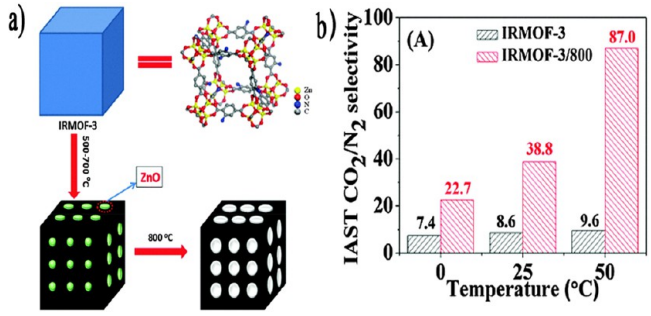

Figure 6. (a) Carbonization of IRMOF-3 and synthesis of N-doped carbon monolith (NCM); (b) enhanced CO_2/N_2 selective adsorption of IRMOF-3/800. (Reproduced with permission from ref 66. Copyright Royal Society of Chemistry, 2016.)

shown that the carbonization temperature has a great impact on the porosity of the resultant product. For example, the N-doped carbon monolith produced under the carbonization temperature of 800 °C (named IRMOF-3/800) has higher porosity than those carbonized at 500−700 °C because of the evolution of the activator (ZnO). Transformation of the structure improves the odds of interacting nitrogen and CO_2. In this way, these N-doped carbon monoliths are believed to be better selective adsorbents of CO_2 than the pristine IRMOF. The result is that IRMOF-3/800 exhibits highly selective CO_2/N_2 adsorption, which is greater than that of pristine IRMOF-3 and even most MOFs (Figure 6b).[66]

2.1.3. IRMOF-6: Adsorption of CO_2, H_2, and Effective Separation for Alkanes. The linkers of MOFs are known to have an influence in the adsorption ability of MOFs. Therefore, the cyclobutenyl group of IRMOF-6 makes its nature of adsorption different from other IRMOFs'.[72] In the field of CO_2 adsorption, early experiments have shown that IRMOF-6 owns the capacity for carbon dioxide that is larger than that of MOF-2, IRMOF-11, and some other MOFs. Concerning the capacity of adsorbing CO_2, the performance of IRMOF-6 is slightly better than that of IRMOF-3 though their pore sizes are similar.[27]

Compared with IRMOF-1 and some conventional adsorbents (such as carbon nanotube), IRMOF-6 has better performance in the storage of hydrogen. This has been

DOI: 10.1021/acs.cgd.9b00879
Cryst. Growth Des. 2019, 19, 7439−7462

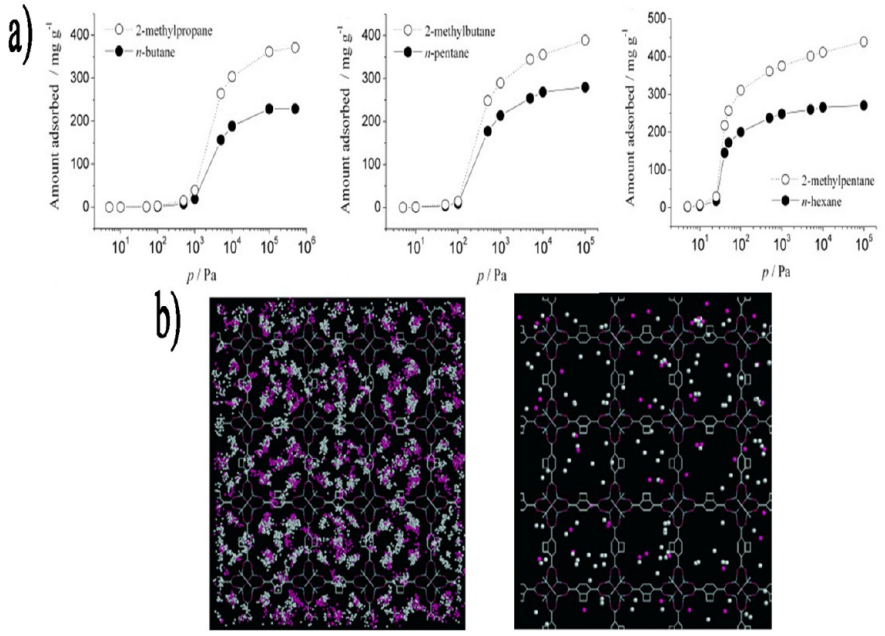

Figure 7. Separation of alkene mixture in IRMOF-6. (a) Adsorption isotherms of different mixtures at ratio of 1:1 in IRMOF-6 (at 298 K). (b) Probability distribution of mixtures containing *n*-butane and 2-methylpropane at a ratio of 1:1 in IRMOF-6 (left: 298 K, 0.5×10^3 kPa. right: 298 K, 0.5×10^{-1} kPa. red: linear alkenes. white: branched alkenes). (Reproduced with permission from ref 67. Copyright John Wiley and Sons, 2007.)

confirmed by the experiment that tested the adsorption of H_2 by IRMOF-1 and IRMOF-6 at room temperature and under a safe pressure (10 bar). The percent uptake of hydrogen by IRMOF-6 is nearly 2-fold that of IRMOF-1 (4.2 H_2 per formula unit for IRMOF-6 and ~1.9 for IRMOF-1).[68]

The introduction of cyclobutenyl groups strengthens the spatial hindrance and brings adjustment to pores of IRMOF-6, which enhances the separation for C_4-C_6 linear and branched alkenes (Figure 7a). With the use of molecule dynamics (MD) and the grand canonical Monte Carlo (GCMC) method, the researchers have discovered that *n*-butane was distributed more widely than 2-methylpropane in metal clusters of IRMOF-6, and the residence time is longer (Figure 7b). A conclusion has been drawn that it is more difficult for C_4-C_6 branched alkenes to get access to the Zn_4O of IRMOF-6 due to cyclobutenyl groups. IRMOF-6 offers the opportunity to be utilized for the separation of an alkene isomer mixture, and it has larger capacities for hydrocarbon than some common inorganic adsorbents (such as silica zeolite).[67]

2.1.4. IRMOF-8: H_2 Storage and C_2H_4/C_2H_6 Separation. IRMOF-8 is a well-studied isoreticular metal−organic framework. The especial linker (2,6-napthalenedicarboxylic acid, 2,6-H_2NDC) of IRMOF-8 influences its performance in sorption and separation. Herein, some applications of IRMOF-8 and its derivatives as sorbents are introduced.

IRMOF-8 has the potential to be a hydrogen and fuel gas storage material due to its adsorption ability of gases of small molecular weight such as hydrogen and methane. The comparison of some properties of IRMOF-8 with other IRMOFs is shown in Table 1. Though the intrinsic surface area and pore volume of IRMOF-8 is lower than those of the three IRMOFs we introduced above, the capacities of IRMOF-8 are quite satisfying. The strong interaction between adsorbates and IRMOF-8 is likely to contribute to such high capacities. For example, the interaction between CH_4 and IRMOF-8 proves to be greater than for some other IRMOFs like IRMOF-1, IRMOF-6, IRMOF-16, and IRMOF-18.[72] The adsorption capacities of IRMOF-8 for H_2 and CH_4 reach 15.0 $mg \cdot g^{-1}$ and 254 $cm^3 \cdot g^{-1}$, respectively, under the given conditions (shown in Table 2.), which are both greater than those of IRMOF-1.[30,56]

Many methods have been reported to make IRMOF-8 more suitable for practical hydrogen storage. Feldblyum et al. prepared non-interpenetrated IRMOF-8 in a room temperature synthesis. Moreover, Orefuwa et al. synthesized IRMOF-8 in a modified solvothermal method in a shorter time than the method that uses a convective oven. Compared to traditional synthesis, these methods can not only increase the efficiency but also produce IRMOF-8 with similar or even enhanced hydrogen capacity.[81,82] Some other methods focus on enhancing the hydrogen storage of IRMOF-8 by combining the MOF with other materials. As we mentioned above, Li and Yang have utilized hydrogen spillover of IRMOF-8 with the purpose of enhancing the hydrogen storage of IRMOF-8. Furthermore, they have utilized sucrose as the precursor for bridged hydrogen spillover, and the reported hydrogen capacities are up to 1.8 and 4 wt % at 298 K and 10 MPa, which are obviously higher than that of pristine IRMOF-8 (0.5 wt %).[29,70] In addition, C atom of the organic linker and CO_2 group of IRMOF-8 are found to play significant roles in storing hydrogen.[75] However, it is necessary to note that Ardelean et al. prepared IRMOF-8 bridged and unbridged composites with the use of a Pt/AC catalyst by following the above-mentioned method, but the enhancement of hydrogen storage was not reproduced.[83] There is still development space for applications of IRMOF-8 in hydrogen storage.

Materials for separation of ethylene from ethane are of great significance in the petrochemical industry. The lack of unsaturated metal sites and two adjacent aromatic rings of IRMOF-8 makes it advantageous in adsorbing ethane over ethylene. This has been confirmed by a flow experiment, in which the mixture of ethane and ethylene is passed in a IRMOF-8 filled column. As a consequence, ethylene was obtained first out of the IRMOF-8 filled column and the

DOI: 10.1021/acs.cgd.9b00879
Cryst. Growth Des. 2019, 19, 7439−7462

selectivity values varied from 3.4 to 1.6 depending on temperature and pressure (Figure 8).[71] The intrinsic structure

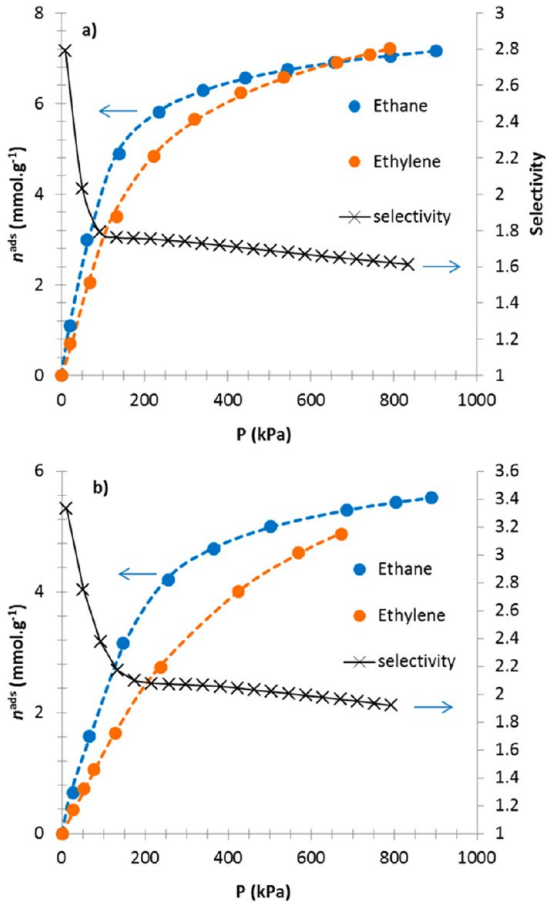

Figure 8. Adsorption isotherms of C_2H_6 and C_2H_4 and selectivity values at different temperatures (a: 298 K, b: 318 K) that confirm the selective adsorption of ethane and ethylene by IRMOF-8. (Reproduced from ref 71.)

of IRMOF-8 leads to different interactions between the MOF and other organic compounds such as ethane and ethylene, which makes it possible to apply IRMOF-8 to separate specific components from the mixture.

2.2. Catalysts. *2.2.1. IRMOF-1.* Acting as catalysts for many chemical reactions is another significant application of metal–organic frameworks. As is known to us, plenty of MOFs can be synthesized nowadays by choosing various metal centers and organic ligands. Different kinds of catalytic active sites make the MOFs promising catalysts for numerous reactions. The porosity of MOFs provides them with the potential to be employed as catalysts by modifications.[84] There are many methods for expanding the application of MOF in catalysis such as doping with metal catalyst[85,86] and post-synthesis modification (PSM).[87,88]

Ever since the origin of IRMOFs, many efforts have been made to utilize them in effective and efficient catalysis. For IRMOF-1, there has been much research focused on the applications in catalysis. For example, the IRMOF-1 derived carbon deposited with Cu nanoparticles can be a high performance catalyst for multicomponent synthesis of propargylamines,[89] and IRMOF-1 supported Pt nanoparticles are able to catalyze the reaction of furfural with ethanol.[90] Moreover, the derivatives of IRMOF-1 show good catalytic performance in Knoevenagel condensation[91] and oxygen reduction reaction (ORR).[92] Herein, the new advances in utilizing IRMOF-1 in photocatalysis and catalysis of Friedel–Crafts alkylation are introduced (Table 4).

Table 4. Some Applications of IRMOF-1, IRMOF-3, and Their Derivatives in Catalysis

IRMOF	catalyst	reaction type	ref
IRMOF-1	BiOBr/MOF-5(IL)	Photocatalytic degradation of methyl orange	52
	HOQ@MOF-5	Photocatalytic degradation of phenyl	93
	MOF-5@SBA-15	Friedel–Crafts alkylation of benzyl bromide with toluene	76
	hybrid material of IRMOF-1 and attapulgite	Friedel–Crafts alkylation of benzyl bromide with toluene	77
IRMOF-3	F-IRMOF-3	the coupling reaction of carbon dioxide with propylene oxide	94
	IRMOF-3-PA-Cu	O-arylation reactions of aryl alcohols with aryl bromides	95
	NPCNH2-MIL-53	the activation of peroxymonosulfate (PMS)	96
	IRMOF-3(Mem)	Knoevenagel condensation reaction between benzaldehyde and ethyl cyanoacetate	97
	IRMOF-3/Fe_3O_4	Knoevenagel condensation reaction between benzaldehyde and ethyl cyanoacetate	98
	$CoFe_2O_4$@SiO_2@IRMOF-3	the synthesis of functionalized dihydro-2-oxopyrroles	99

2.2.1.1. Photocatalysts. Due to the energy crisis, utilizing renewable clean energy such as light energy has been a hot topic for a long period of time. Research in IRMOF confirms that it can play an important role in the utilization of light energy. The choice of semiconductor is crucial for synthesizing photocatalysts. Bismuth oxybromide (BiOBr) is a bismuth oxyhalide which is proven to have a good response for visible light. However, the low conduction band position and low surface area of directly synthesized particles limit the applications of BiOBr in photocatalysis. Innovation in the synthesis of IRMOF-1 has improved the photocatalysis performance of BiOBr. Different from the other methods for synthesizing IRMOFs that we introduced in detail in this Review (such as solvothermal methods), Yang et al. have utilized an electrochemical method to synthesize IRMOF-1 in the ionic liquid (IL) environment, and the product is named MOF-5(IL). Through mixing MOF-5(IL) with BiOBr and the other following process, the researchers have obtained a BiOBr/MOF-5(IL) composite. The degradation of methyl orange (MO) has been used for testing the photocatalytic of BiOBr/MOF-5(IL), and the MO degradation ratio for it reaches 87.9% in the condition of simulated solar-light irradiation (58.1% for pure BiOBr). This result confirms that IRMOF can replace noble metal in enhancing the property of bismuth oxyhalide in photocatalysis. Further investigation reveals that $\cdot O_2^-$ and H^+ play important roles in the degradation of MO. The separation of hole and electron and the formation of hydroxyl radicals can be promoted in the BiOBr/MOF-5(IL) system, and the MOF is able to speed up production of $\cdot O_2^-$. Therefore, the synergistic effect of MOF-5(IL) and photosensitized BiOBr enhances the photocatalytic activity of BiOBr/MOF-5(IL).[52]

DOI: 10.1021/acs.cgd.9b00879
Cryst. Growth Des. 2019, 19, 7439–7462

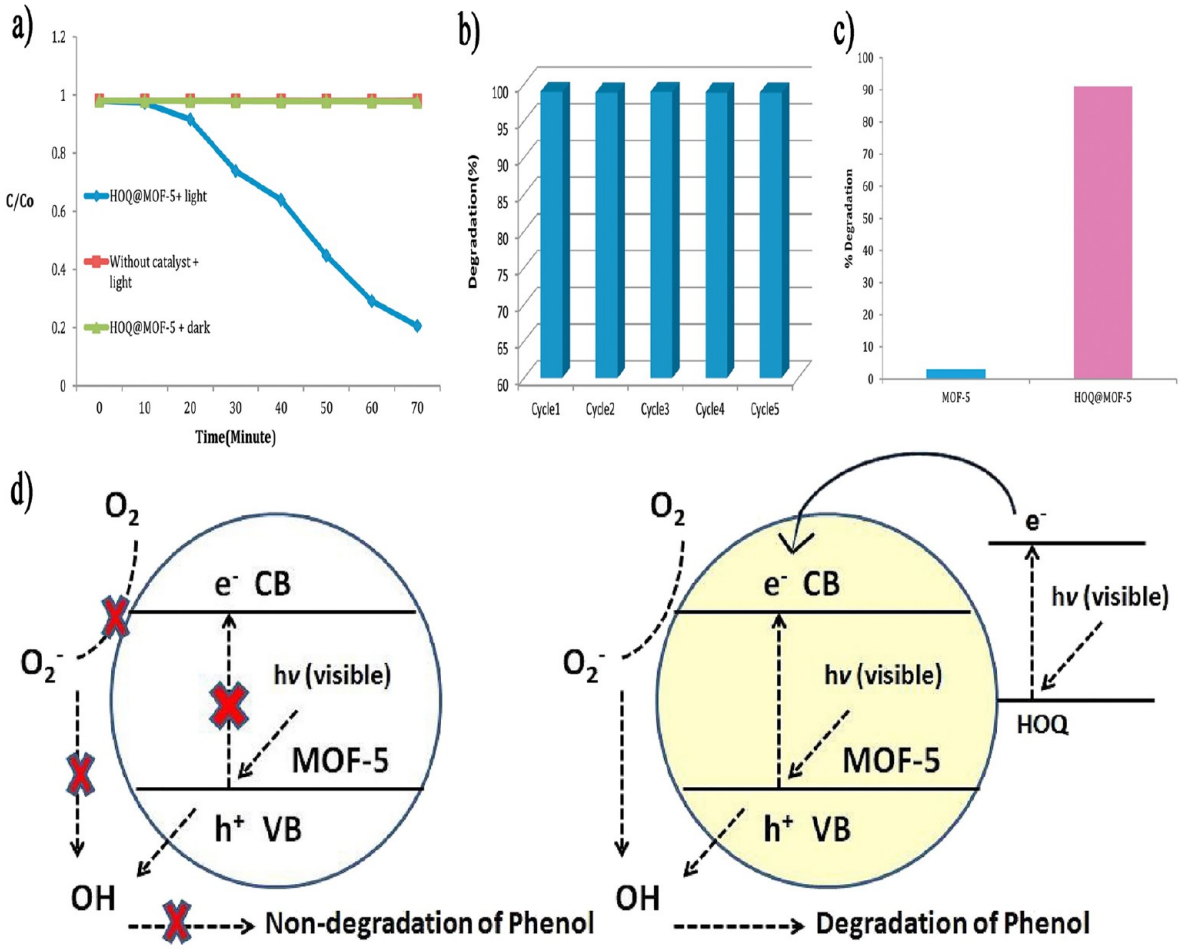

Figure 9. (a) HOQ@MOF-5 acts as a photocatalyst for degradation of phenol; (b) stability of HOQ@MOF-5 as a photocatalyst; (c) HOQ@MOF-5 shows higher catalytic efficiency than pristine MOF-5; (d) illustration of degradation catalyzed by HOQ@MOF-5. (Reproduced with permission from ref 93. Copyright Elsevier, 2018.)

According to some earlier reports, IRMOF-1 can act as a semiconductor when exposed to visible light. In addition, M-IRMOF-1 (M = Ca, Mg, Be, and Cd), which are obtained by changing metal clusters of IRMOF-1, have similar band gaps as IRMOF-1. The photocatalytic activity can be different when the organic linkers of IRMOFs vary, which has been verified by the photooxidation of propene.[100] These observations also indicate that IRMOFs own the potential in the field of photocatalysis. Nowadays, synthesizing composite materials by using IRMOF and sensitizers that absorb light (such as 8-hydroxyquinoline, abbreviated as HOQ) is a practical way to utilize IRMOFs. Based on this principle, HOQ@MOF-5 has been synthesized and the photocatalytic performance of HOQ@MOF-5 has been tested through the photocatalytic degradation reaction of phenyl (Figure 9). In the experimental condition where the initial concentration of the reactant was 1 mmol and the reaction time was 40 min, the degradation ratio by HOQ@MOF-5 was 91%. The comparison of degradation of phenyl catalyzed by various photocatalysts shows that the performance of HOQ@MOF-5 is excellent (shown in Table 5).[93]

2.2.1.2. Catalysts for Friedel–Crafts Alkylation. Friedel–Crafts alkylation is one of the most important substitutions of aromatic compounds. The application of IRMOF-1 in Friedel–Crafts alkylation of aromatic compounds has been explored and some advances have been made. The coordination-unsaturated open metal sites of IRMOF-1 imply that it could be a catalyst for the Friedel–Crafts alkylation reaction of aromatic compounds, which is often catalyzed by Lewis acids.[76,104,105] However, the catalytic performance of pure IRMOF-1 is not ideal enough. As a matter of fact, one way to improve the catalytic performance of MOF is reducing the size of the MOF crystal. Inspired by this, a unique double-solvent strategy has been utilized to synthesize IRMOF-1 within the pores of a mesoporous silica, which is named SBA-15 (Figure 10a). The use of a hydrophilic solution and hydrophobic solvent makes this strategy different from the traditional methods by which the bulk IRMOF-1 is obtained. Growing IRMOF-1 crystals in silica mesopores reduces the size of the crystals in order to increase the accessibility of reactant to the active sites of IRMOF-1. As a result, MOF-5@SBA-15 shows enhanced performance in catalyzing the Friedel–Crafts alkylation reaction of benzyl bromide with toluene (Figure 10c). The conversion of benzyl bromide is 100% after 3 h using MOF-5@SBA-15 as catalyst.[76]

Another method to synthesize an effective catalyst of Friedel–Crafts alkylation is hybridizing IRMOF with a natural material. One of representative experiments is hybridization of IRMOF-1 with attapulgite, which is a well-studied silicate mineral (Figure 10b). Attapulgite is easy available and economic, which makes it advantageous over other commonly used materials such as carbon nanotubes. Some reports have

DOI: 10.1021/acs.cgd.9b00879
Cryst. Growth Des. 2019, 19, 7439–7462

Table 5. Comparison of Catalytic Performance of Materials Based on IRMOF-1 and IRMOF-3 with Other Catalysts

reaction type	catalyst	conversion rate	experiment condition	substrate concentration	ref
Photocatalytic degradation of methyl orange	BiOBr/MOF-5(IL)	87.9%(Degradation ratio of MO)	150 min (simulated solar light irradiation)	-	52
	pure BiOBr	58.1%(Degradation ratio of MO)	150 min (simulated solar light irradiation)	-	52
Photocatalytic degradation of phenyl	HOQ@MOF-5	91% (photoconversion rate of phenol)	40 min (irradiation)	1 mmol	93
	HOQ@TiO_2	68% (photoconversion rate of phenol)	5 h (irradiation)	1 mmol	93,101
	Ag_TiO_2	87% (photoconversion rate of phenol)	2 h (irradiation)	15 mg/L phenol	102
	TiO_2	75% (photoconversion rate of phenol)	2 h (irradiation)	15 mg/L phenol	102
Friedel−Crafts alkylation reaction of benzyl bromide with toluene	Pure IRMOF-1	61% (conversion rate of benzyl bromide)	80 °C, 3 h	12.4 mmol (benzyl bromide), 37.3 mmol (toluene)	76
	MOF-5@SBA-15	100% (conversion rate of benzyl bromide)	80 °C, 3 h	12.4 mmol (benzyl bromide), 37.3 mmol (toluene)	76
	hybrid material of IRMOF-1 and attapulgite (MA-3, MA-4)	99%-100% (conversion rate of benzyl bromide)	80 °C, 2 h	12.4 mmol (benzyl bromide), 37.3 mmol (toluene)	77
the coupling reaction of carbon dioxide with propylene oxide	F-IRMOF-3-4d	98% (the yield of propy- lene carbonate)	140 °C, 1.5 h	500 mmol (PO), initial CO_2 pressure 2 MPa	94
	MOF-5/n-Bu4NBr	97.6% (the yield of propy- lene carbonate)	50 °C, 4 h	PO(20 mmol) with 2.5 mol % ammonium salts, initial CO_2 pressure 6 MPa	103
Knoevenagel condensation reaction ofbenzaldehyde and ethyl cyanoacetate	S-IRMOF-3(Mem)	87% (conversion rate of ethyl cyanoacetate)	333 K, 4 h	1.6 mmol·mL^{-1} of benzaldehyde,1.4 mmol·mL^{-1} of ethyl cyanoacetate	97
	M-IRMOF-3(Mem)	46%(conversion rate of ethyl cyanoacetate)	333 K, 4 h	1.6 mmol·mL^{-1} of benzaldehyde,1.4 mmol·mL^{-1} of ethyl cyanoacetate	97
	FI-3	98.3% (conversion rate of ethyl cyanoacetate)	333 K, 4 h	1.6 mmol·ml^{-1} of benzaldehyde,1.4 mmol·mL^{-1} of ethyl cyanoacetate	98

DOI: 10.1021/acs.cgd.9b00879
Cryst. Growth Des. 2019, 19, 7439−7462

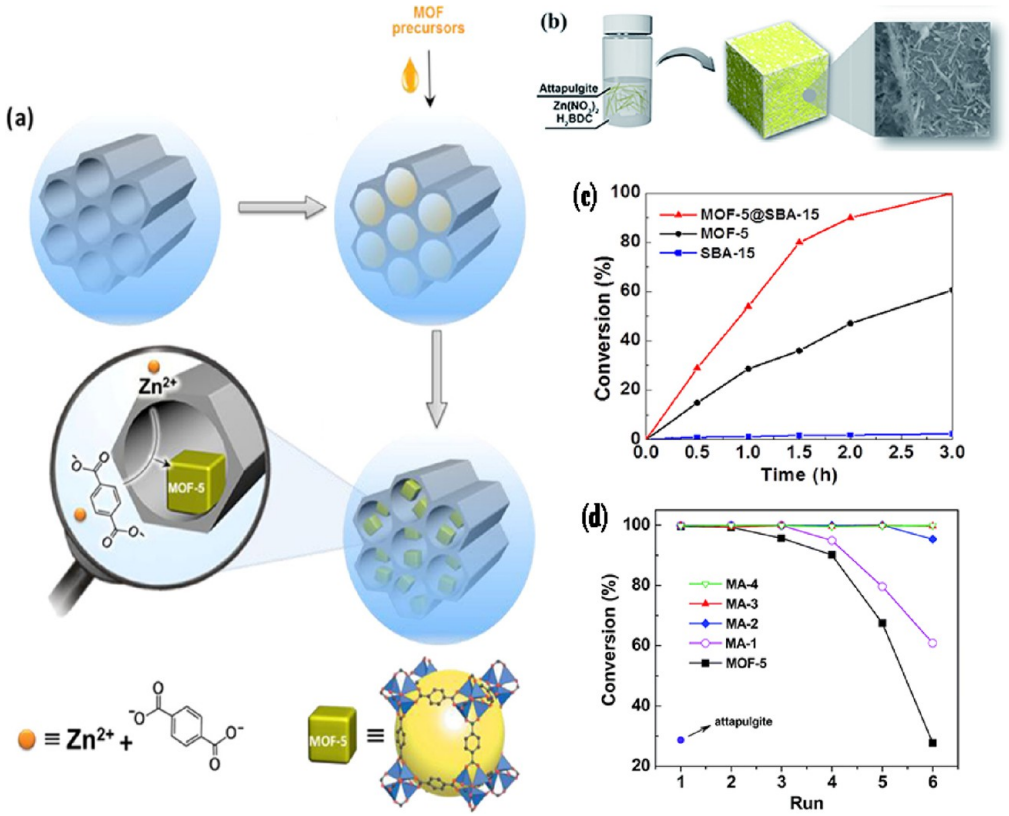

Figure 10. Applications of IRMOF-1 in catalyzing Friedel−Crafts alkylation of benzyl bromides with tolune. Illustration of synthesis of (a) MOF-5@SBA-15 and (b) hybrid materials MA-*n* and excellent catalytic performances of (c) MOF-5@SBA-15 and (d) MA-*n*. (a and c: Reproduced from ref 76. b and d: Reproduced with permission from ref 77. Copyright Royal Society of Chemistry, 2015.)

shown that fabrication of catalysts with unique catalytic performance and high stability can be realized by combining MOFs with natural clay attapulgite. For example, Cu-BTC hybridized with natural clay attapulgite and material obtained by incorporation of functionalized attapulgite into the MOF HKUST-1 show enhanced hydrothermal stability and catalytic activity for the styrene oxide ring opening.[106,107] The hybrid materials prepared by hybridizing IRMOF-1 with attapulgite are named MA-*n*. MA-*n* owns higher hydrostability and better performance in catalyzing Friedel−Crafts alkylation of benzyl bromide with toluene (Figure 10d). The contents of attapulgite of MA-1 to MA-4 are 4.0, 8.3, 16.5, and 16.5 wt %, respectively. Compared with pure IRMOF-1, the hybrid materials are more efficient and catalytically stable. After six runs and recovery of activity, the conversion still reaches 100% with the catalysis of hybrid material.[77]

2.2.2. IRMOF-3. Introduction of basic groups such as the $-NH_2$ group into MOFs is a practicable way to prepare basic catalysts. MOF-derived solid bases can be excellent catalysts for many important chemical reactions including Aldol condensation, Michael addition, and Knoevenagel condensation.[108,109] The uncoordinated amine moieties make the modification of IRMOF-3 easier to realize, and many advances in converting pure IRMOF-3 into efficient and effective catalysts in the chemical industry have been made. To the best of our knowledge, the methods to synthesize catalysts based on IRMOF-3 are quite different from those for IRMOF-1. Herein, we have demonstrated a summary of the representative work in improving the catalytic performance of IRMOF-3.

2.2.2.1. Catalysts Fabricated by PSM of NH_2-Containing IRMOF-3. Post-synthesis modification (PSM) can not only enhance the adsorption ability of IRMOF-3 but also be used to develop functionalized IRMOF-3 as catalysts. By treating as-synthesized IRMOF-3 with methyl iodide (CH_3I), the functionalized IRMOF-3 (named F-IRMOF-3) is obtained. The procedure is shown in Figure 11a. This product of post-synthesis modification shows excellent catalytic activity for the coupling reaction of carbon dioxide with propylene oxide (abbreviated as PO), in which propylene carbonate is yielded. Unlike the low yield of the desired product when IRMOF-3 and methyl iodide are used as the catalysts respectively, the yield with functionalized IRMOF-3 as heterogeneous catalyst is 89−98%. Furthermore, the catalytic activity is related to the functionalization time. The catalytic performance of functionalized IRMOF-3 is improved with the time of functionalization added.[94] IRMOF-1 has also been used as a catalyst for the coupling reaction of carbon dioxide with propylene oxide with the existence of different kinds of quaternary ammonium salts.[103] The performance of F-IRMOF-3 is compared with this synergetic catalyst in Table 5. Otherwise, the reusability of F-IRMOF-3 has been confirmed (Figure 11b). The Zn_4O clusters and $-NH_2$ groups of IRMOF-3 are able to activate the epoxy ring. I^- in F-IRMOF-3 can open the epoxy ring. Therefore, the synergistic effect of metal clusters, $-NH_2$ groups, and I^- makes F-IRMOF-3 a catalyst for the synthesis of cyclic carbonates with improved performance. However, the instability in moist air hinders the process of exploiting this catalyst.[94] This problem might be resolved by extending methods for enhancing hydrostability of IRMOF-1.

Post-synthetic modification of IRMOF-3 has been developed into a series of facile processes. The copper-catalyzed O-arylation method is one of the most important ways to produce

DOI: 10.1021/acs.cgd.9b00879
Cryst. Growth Des. 2019, 19, 7439−7462

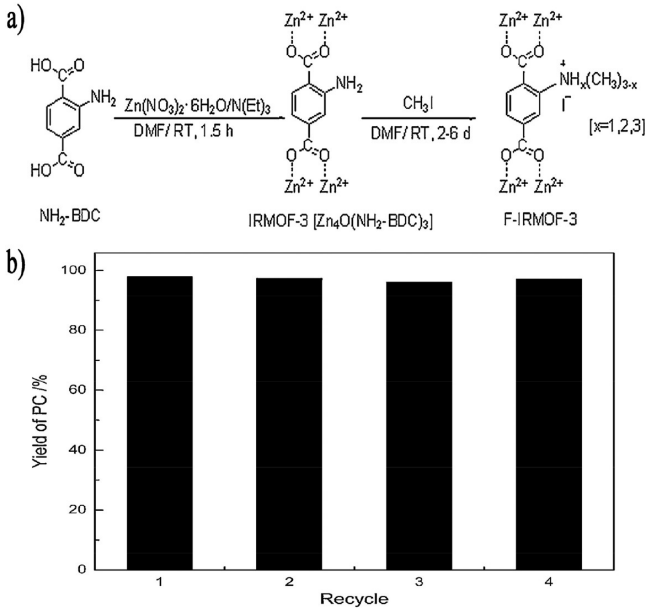

Figure 11. (a) Preparation of F-IRMOF-3 and (b) high yield of propylene carbonate (PC) and recyclability of F-IRMOF-3-4d. (F-IRMOF-3-4d is F-IRMOF-3 with the functionalization time of 4 days.) (Reproduced with permission from ref 94. Copyright Elsevier, 2012.)

diaryl ethers. In order to anchor copper(II) into IRMOF-3 and apply IRMOF-3 in catalysis, multistep post-synthetic modification of IRMOF-3 has been undertaken. After treating IRMOF-3 with pyridine-2-aldehyde, the obtained IRMOF-3-PA is stirred with $CuCl_2 \cdot 2H_2O$. By the following treatment, IRMOF-3-PA-Cu has been synthesized (Figure 12a). IRMOF-3-PA-Cu is tested to be an effective and reusable catalyst for O-arylation reactions, in which aryl alcohols react with aryl bromides to produce various diaryl ethers (Figure 12b). Additionally, the shape selectivity in the product of this recoverable heterogeneous catalyst makes it more attractive. In other words, the yields of products are dependent on their sizes with the application of IRMOF-3-PA-Cu.[95]

The utilization of doped carbon materials in catalysis is emerging nowadays. The sources of these doped carbon materials include natural substances and MOFs.[110−112] For instance, they act as catalysts in activating peroxymonosulfate (PMS). As a consequence, hydroxyl radical (·OH) and sulfate radical ($SO_4^{\cdot-}$) are yielded. High surface areas and porosity of MOFs make them attractive for synthesizing nanocarbon materials. Nitrogen-doped porous carbon ($NPC_{IRMOF-3}$) has been obtained by carbonization of IRMOF-3 at various temperatures and shows an instinct in catalyzing the activation of peroxymonosulfate (PMS). The characterization of different kinds of NPC prepared in similar ways is shown in Figure 13a,b. The yield of hydroxyl radical and sulfate radical indicates that the $NPC_{IRMOF-3}$/PMS system could be used for removing organic pollutants such as phenol and methyl orange (Figure 13c,d). $NPC_{IRMOF-3}$ has better catalytic performance than Co^{2+}, which is a catalyst with high efficiency for activating PMS. Compared among the products of carbonization of MOFs, $NPC_{IRMOF-3}$ is also a promising catalyst. The nitrogen species (pyridinic N, pyrrolic N, and graphitic N) prove to influence the catalytic activity of NPC. Among them, the graphitic N plays a key role in activation of PMS for the possible reason that it can boost the electron transfer from carbon to oxygen. Therefore, $NPC_{IRMOF-3}$ is a more ideal catalyst than $NPC_{NH2-MIL-53}$ due to its higher graphitic N content (Figure 13e,f).[96]

Synthesizing a MOF membrane in substrate is a research trend in catalytic application of MOFs.[113−116] Bare IRMOF-3 particles have provem to be catalysts for some reactions such as the Knoevenagel condensation reaction between benzaldehyde and ethyl cyanoacetate, which is an important reaction in the chemical industry. The Knoevenagel condensation reaction is

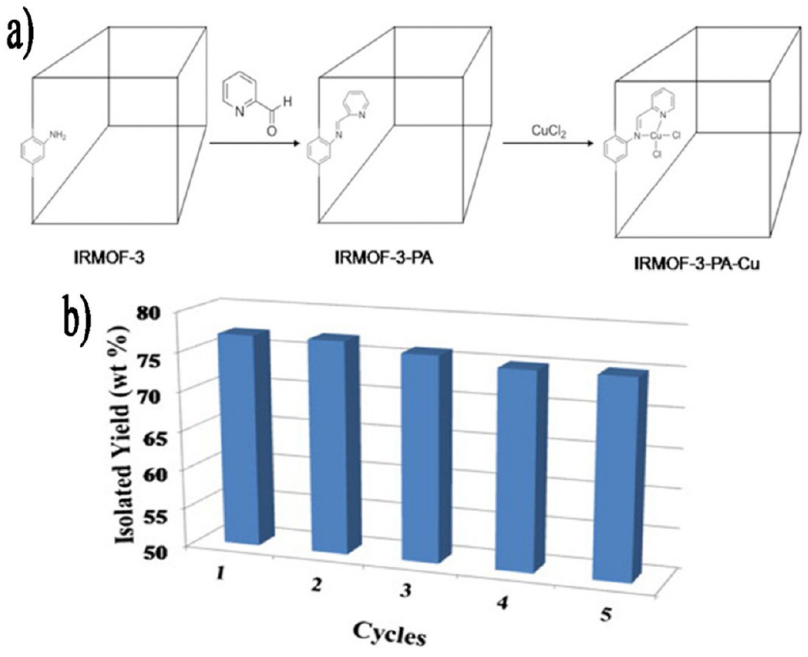

Figure 12. (a) Procedure of synthesis of IRMOF-3-PA-Cu and (b) IRMOF-3-PA-Cu proves to be a reusable and efficient catalyst for O-arylation reaction. (Reproduced with permission from ref 95. Copyright Elsevier, 2015.)

DOI: 10.1021/acs.cgd.9b00879
Cryst. Growth Des. 2019, 19, 7439−7462

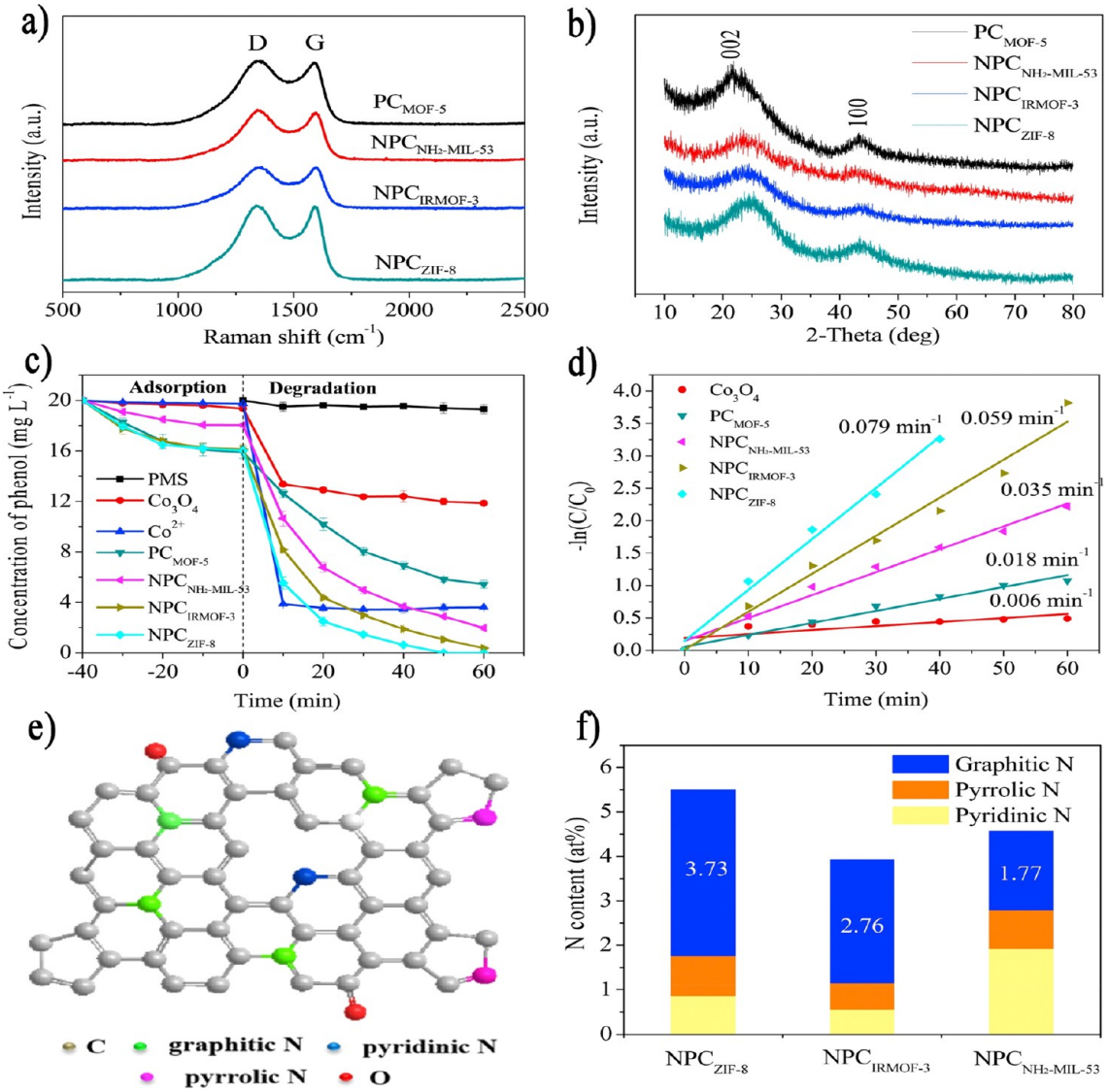

Figure 13. N-Doped porous carbon (NPC) obtained by carbonization of IRMOF-3 can catalyze the activation of peroxymonosulfate. Characterization of different kinds of NPCs (a: Raman spectra, b: X-ray diffraction patterns); (c) comparison of phenol removal on $NPC_{IRMOF-3}$ with other porous carbon materials; (d) phenol degradation rates of $NPC_{IRMOF-3}$ and other candidates; (e) three kinds of nitrogen species in N-doped porous carbon; (f) N content of different NPCs. (Reproduced with permission from ref 96. Copyright Elsevier, 2017.)

also used to test the basic strength of the solid base which catalyzes the reaction.[117] The carboxylate oxygen of IRMOF-3 acts as an electron donor and makes a intramolecular hydrogen bond interaction with amino, which leads to the stronger basicity of the amino group of IRMOF-3 than that of aniline. The enhanced basicity of IRMOF-3 is the reason for its high catalytic activity for the Knoevenagel condensation reaction.[118] Lee et al. utilized the developed sonochemical technique to synthesize the IRMOF-3 membrane on porous Al_2O_3 disk support. The obtained IRMOF-3 membrane has been designated as S-IRMOF-3(Mem). S-IRMOF-3(Mem) exhibits far better catalytic performance than M-IRMOF-3(Mem), which is synthesized by the process of microwave heating (Table 5). M-IRMOF-3(Mem) can not only maintain the nearly high catalytic activity of IRMOF-3 particles synthesized by the similar sonochemical method but also enhances the stability and recyclability.[97]

2.2.2.2. Core−Shell IRMOF-3 Composites as Catalysts. Synthesis of core−shell MOF composites is also an effective way to harness the strength of MOF.[119−122] As a case in point, combining MOFs with small-sized particles can prepare catalysts that meet the actual needs of production. Besides outstanding catalytic performance, the convenience of separating catalyst from reaction system is also a requirement for an ideal catalyst. Core−shell composites with magnetic particles such as Fe_3O_4 and $CoFe_2O_4$ are synthesized, and then the goal of separating catalyst from the reaction system can be achieved by using an external magnetic field. This method has been employed to synthesize IRMOF-3/Fe_3O_4 composites and $CoFe_2O_4$@SiO_2@IRMOF-3.

The core−shell composites IRMOF-3/Fe_3O_4 are improved catalysts for the Knoevenagel condensation reaction between benzaldehyde and ethyl cyanoacetate. The synthesis process of IRMOF-3/Fe_3O_4 is shown in Figure 14a. Several crucial steps of synthesis are (1) adding the mixture containing polyvinylpyrrolidone (PVP), ethanol, and *N*,*N*-dimethylformamide (DMF) into the precursor solution for synthesizing IRMOF-3, (2) adding Fe_3O_4, and ultrasonic treatment. The catalytic

DOI: 10.1021/acs.cgd.9b00879
Cryst. Growth Des. 2019, 19, 7439−7462

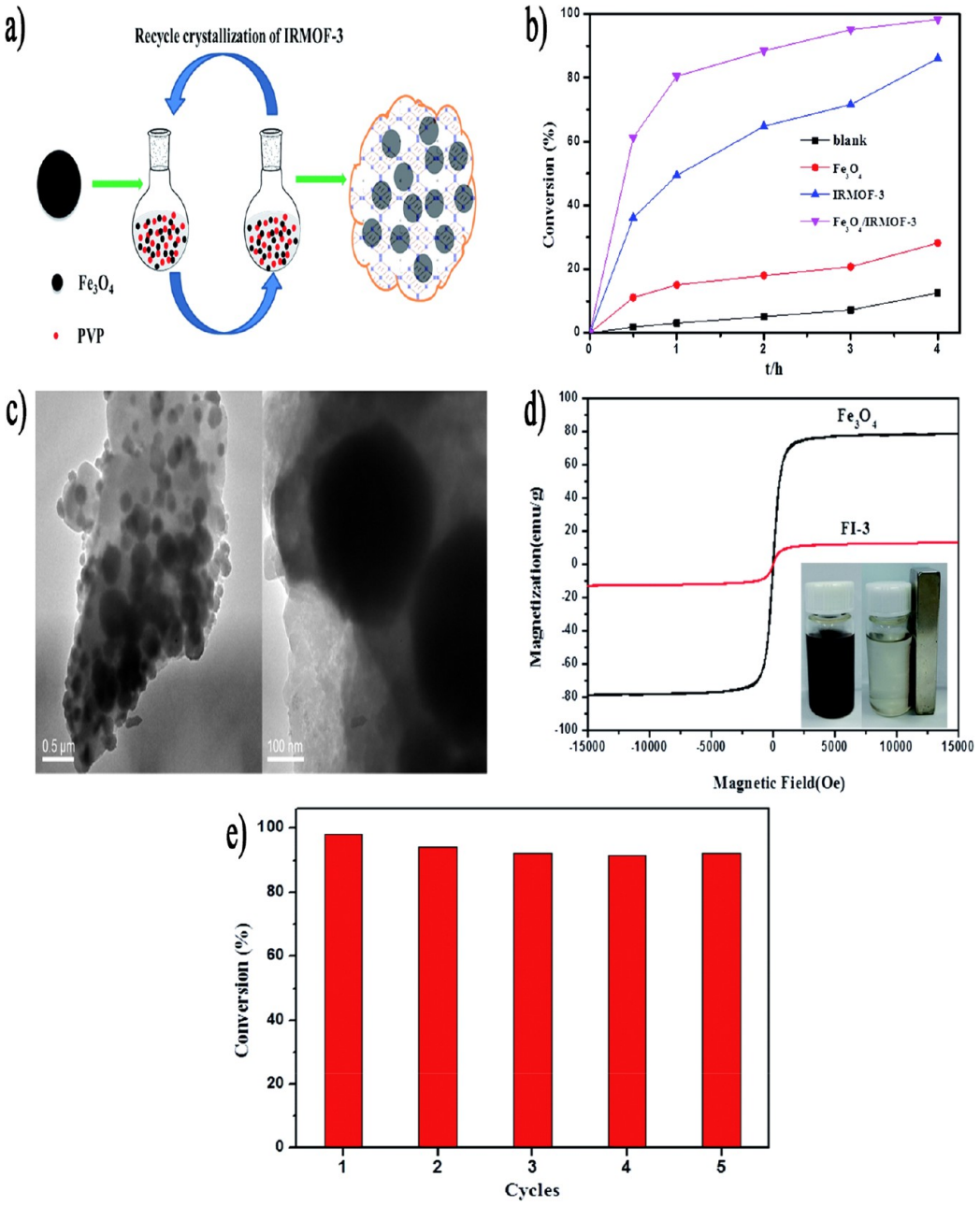

Figure 14. Fe_3O_4/IRMOF-3 works as a catalyst for the Knoevenagel condensation reaction: (a) synthesis of catalyst; (b) conversion of ethyl cyanoacetate in Knoevenagel condensation reaction (catalyst: FI-3, condition: 333 K); (c) transmission electron microscope images of FI-3; (d) magnetic property of FI-3 (inset: illustration of magnetic separation with the use of magnet); (e) limited change of catalytic performance of FI-3 after 5 cycles. (Reproduced with permission from ref 98. Copyright Royal Society of Chemistry, 2016.)

performance of products Fe_3O_4/IRMOF-3 is better than that of Fe_3O_4 as well as IRMOF-3 (Figure 14b) and varies with the time of repetition of synthesis. FI-3 refers to products that go through three cycles of synthesis. With the adjustment of temperature and catalyst dosage, the conversion of ethyl cyanoacetate in the presence of FI-3 can be 100%. The TEM image and magnetic property of FI-3 are also shown in Figure 14c,d. In addition, the slight decrease of conversion of reactants indicates that FI-3 has excellent recyclability (Figure 14e).[98]

Based on a similar principle, $CoFe_2O_4$@SiO_2@IRMOF-3 has been synthesized by modifying $CoFe_2O_4$ with a SiO_2 layer and depositing IRMOF-3 on the microsphere of $CoFe_2O_4$@SiO_2. The $CoFe_2O_4$@SiO_2@IRMOF-3 is able to effectively catalyze the synthesis of functionalized dihydro-2-oxopyrroles, which is a one-pot reaction. A series of synthesis reactions with the variation of reactants has been used to test the activity of this core−shell composite. The yields for all are more than 80% in the experimental condition. In addition, $CoFe_2O_4$@SiO_2@IRMOF-3 is easy to separate and reuse.[99]

2.3. Sensors. *2.3.1. IRMOF-1.* The utilization of MOFs is one of the most significant trends in sensing and detecting. The superb stability, large surface area, and tunable pore size of MOFs have inspired researchers to utilize MOFs and their derivatives to fabricate keen, selective, and stable sensors. These sensors are promising in applications detecting organic contaminant, biotic component, heavy metal ions, and so forth.

DOI: 10.1021/acs.cgd.9b00879
Cryst. Growth Des. 2019, 19, 7439−7462

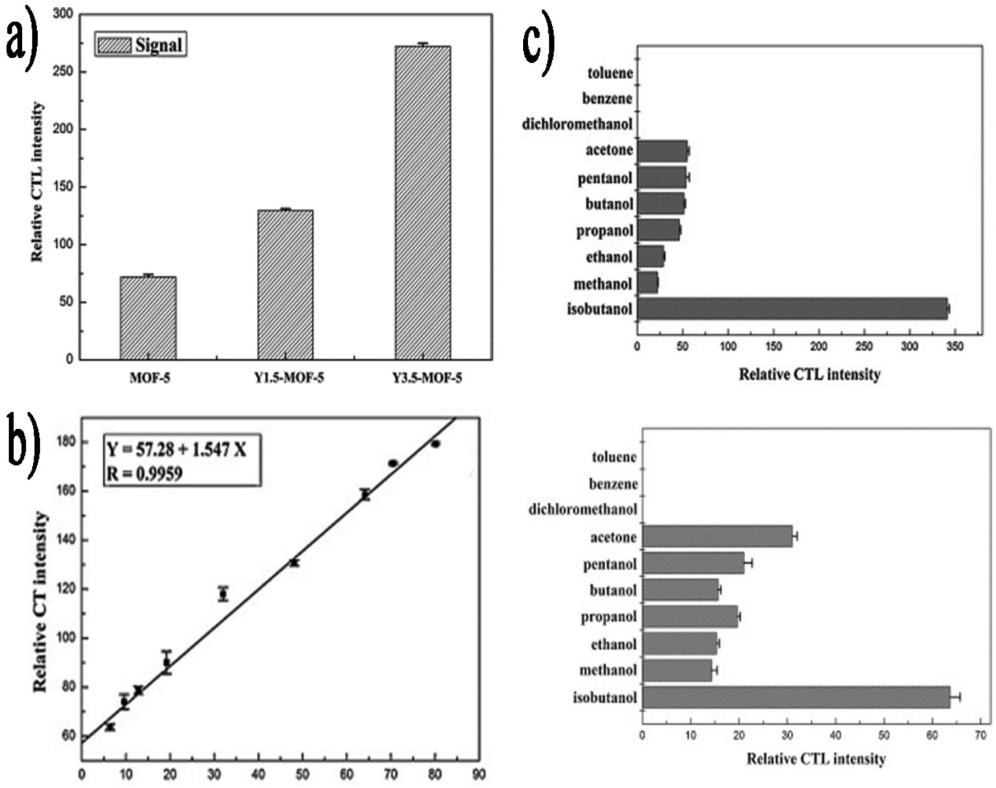

Figure 15. (a) Enhanced CTL intensity of Y-doped IRMOF-1 (Y1.5-MOF-5 and Y3.5-MOF-5 refer to Y-doped MOF-5 whose molar ratios (Y:Zn) are 1.5%:98.5% and 3.5%:96.5%, respectively); (b) the calibration curve shows linear variation of CTL intensity of Y3.5-MOF-5 with the concentration of isobutanol; (c) comparison of CTL emission of ten volatile organic compounds (VOCs) on Y3.5-MOF-5 (top) with pure MOF-5 (bottom). (Reproduced with permission from ref 124. Copyright Elsevier, 2014.)

2.3.1.1. Fluorescent IRMOF-1 Based Sensors for Isobutanol and Heavy Metal Ions. Numerous strategies for applications of IRMOFs in sensing and detection have been put forward. Besides the advantages mentioned above, the fluorescence of IRMOF-1 and IRMOF-3 endows them with great potential in sensing. The mechanism of fluorescence of IRMOF-1 has been revealed to be the good coplanarity of benzene and six-membered Zn−O−C rings in excited as well as ground states.[123] Based on the principle of cataluminescence (CTL), IRMOF-1 has been doped with yttrium, a rare earth element. The CTL emission has been observed with isobutanol passing through the surface of obtained Y-doped IRMOF-1. Compared with undoped IRMOF-1, the CTL intensity of Y-doped IRMOF-1 is improved because Y^{3+} can catalyze the oxidation of isobutanol (Figure 15a,c). Moreover, the CTL intensities have proven to depend linearly on the concentration of isobutanol in a specific range, and the limit of detection (abbreviated as LOD) is low (3.7 mg L^{-1}) (Figure 15b). Therefore, the Y-doped IRMOF-1 is an excellent sensor that can be used to determine isobutanol.[124]

The composite materials based on IRMOF-1 can also play important roles in the field of detecting heavy metal ions. Excess heavy metal ions that exist in bodies of water cause harm to human health. Therefore, effective and sensitive detection of heavy metal ions is of great significance. Several fluorescence sensors for heavy metal ions have been fabricated with the use of IRMOF-1 including mixed matrix membranes (abbreviated as MMMs) incorporated with IRMOF-1 and $CH_3NH_3PbBr_3$@MOF-5 composites.

To synthesize MMMs, a priming method has been utilized and IRMOF-1 particles are mixed with sulfonated poly(arylene ether nitrile) (SPEN) in this process. The basic steps are shown in Figure 16a. Benefiting from the high thermal stability and fluorescent nature of IRMOF-1, the MMMs incorporated with a small amount of IRMOF-1 exhibit improved fluorescence emission over the neat one. It is known that some heavy metal ions play the role of fluorescence quenchers and some probes based on this principle have been fabricated.[125−127] Cu^{2+} has been found to have an apparent fluorescence quenching effect for mixed matrix membranes incorporated with IRMOF-1. The negligible interference from analogues such as Mg^{2+}, Na^{+}, Hg^{2+}, and Zn^{2+} further confirms the applicability of MMMs incorporated with IRMOF-1 as selective sensors for trace level Cu^{2+} (Figure 16b).[128]

The role that IRMOF-1 plays in $CH_3NH_3PbBr_3$@MOF-5 composites is quite different from that in MMMs. One of the hindrances to employ $CH_3NH_3PbBr_3$, a hybrid organic−inorganic halide perovskites, is that $CH_3NH_3^{+}$ is unstable. To overcome this problem, IRMOF-1 has been chosen as matrix material to encapsulate $CH_3NH_3PbBr_3$QDs (i.e., $CH_3NH_3PbBr_3$ quantum dots). Specifically, $PbBr_2$@MOF-5 was obtained by solvothermal methods and was subsequently reacted with CH_3NH_3Br ethanol solution (Figure 17a). It is noteworthy that perovskite QDs own luminescent properties and so does the composite (Figure 17b). The $CH_3NH_3PbBr_3$@MOF-5 composite has been considered as sensors for several heavy metal ions such as Fe^{3+}, Al^{3+}, Bi^{3+}, Cd^{2+}, Co^{2+}, and Cu^{2+} because of the different luminescent responses. The consistently impressive performances in various pH values, enhanced thermal stability, and water resistance make this sensor more useful in detection of heavy metal ions in real aqueous solution (Figure 17c,d).[129]

DOI: 10.1021/acs.cgd.9b00879
Cryst. Growth Des. 2019, 19, 7439−7462

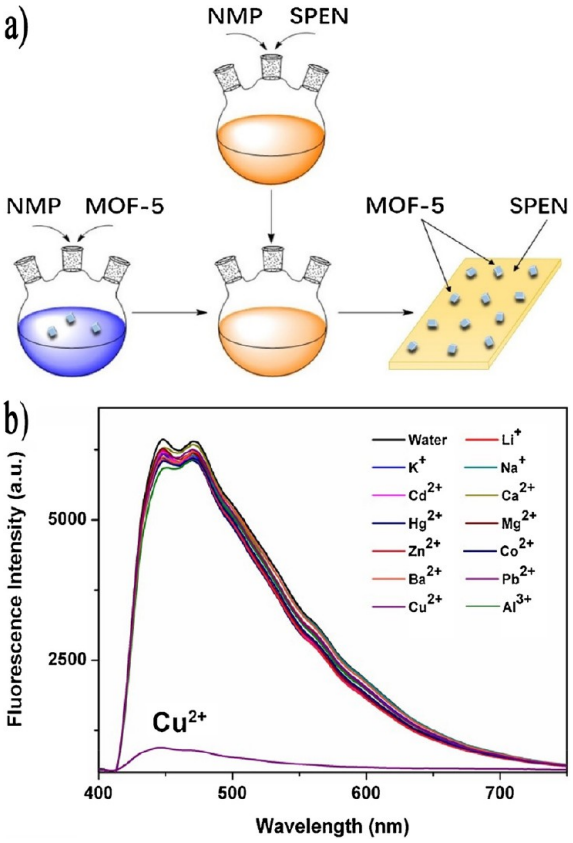

Figure 16. (a) Basic steps of fabricating mixed matrix membranes (MMMs); (b) selectivity of MMMs that are incorporated with 8 wt % IRMOF-1 on detecting Cu^{2+}. (Reproduced with permission from ref 128. Copyright Elsevier, 2018.)

2.3.1.2. IRMOF-1 Based Electrochemical Sensor and Microgravimetric Sensor. IRMOF-1 and its derivatives have also been applied as electrochemical sensors and microgravimetric sensors. Reduced graphene oxide (rGO), poly(diallydimethylammonium chloride) (PDDA), nickel nanoparticle, and IRMOF-1 have been used to synthesize MOF-5@PDDA-rGO-Ni (abbreviated as MOF-5@PGN). Furthermore, methylene blue (MB) encased MOF-5@PGN nanocomplex has been prepared by incorporating MB molecules into IRMOF-1. By depositing MOF-5@PGN and MB encased MOF-5@PGN, respectively, onto the surface of glassy carbon electrode (GCE), two electrochemical sensors for echinacoside have been fabricated. The excellent adsorption capability of IRMOF-1 is beneficial to the sensitive response of these voltammetric sensors. MB encased MOF-5@PGN/GCE has more ideal properties, which is confirmed by the wider linear range as well as lower LOD for echinacoside (Figure 18a).[130] Lv et al. inkjet-printed ink that contained IRMOF-1 crystal on a resonant microcantilever and thus synthesized a microgravimetric sensor for trace amounts of aniline, a carcinogenic substance. Figure 18b is the SEM image of this microgravimetric sensor. IRMOF-1 is known to adsorb aniline and the mass varies during the adsorption. Owing to this nature of IRMOF-1 and unique structure of microcantilever, the sensor can transform mass addition to the signal of frequency shift (Figure 18c). Moreover, this sensor owns outstanding sensitivity and repeatability. The little change in response of tests in a given time period also confirms that it is long-term stable (Figure 18d).[131]

2.3.2. IRMOF-3: Luminescent Sensors Based on IRMOF-3. Nanoscale IRMOF-3 is a promising material in sensing and it has been synthesized on the industrial scale in different ways including the hydrothermal method and the electrochemical method. The pure nanoscale IRMOF-3 prepared by the hydrothermal method is a selective fluorescent sensor for glucose and Fe^{3+} ions with LOD of 0.56 μM and 4.2 nM respectively under the experimental conditions. Furthermore, IRMOF-3 prepared in this way can be used for visual detection of glucose and Fe^{3+} ions (Figure 19a).[132] The electrochemical synthetic method has successfully realized the rapid fabrication of nanoscale IRMOF-3. It has been reported that the obtained nanoscale IRMOF-3 has an enhanced fluorescent response for 2,4,6-trinitrophenol (TNP) than that prepared by the solvothermal method. The nanoscale IRMOF-3 with high crystallinity exhibits LOD for TNP (0.1 ppm), which signifies that nanoscale IRMOF-3 synthesized by the electrochemical method is an improved sensor for TNP (Figure 19b,c). Compared with other nitro explosives such as nitrobenzene (NB) and *p*-nitrotoluene (4-NT), the higher value of $(I_0/I) - 1$ indicates that TNP has more distinct fluorescence quenching effect (Figure 19d). In addition, the mechanism is inferred from cooperation of the electron transfer effect and the fluorescence inner filter effect.[133]

The fluorescent IRMOF-3 has also been employed as a sensor for biorecognition. The pendent amine group of IRMOF-3 plays a significant part in bioconjugating with receptors such as bacteriophages. An optosensor bacteriophage/IRMOF-3 has been prepared by immobilizing a bacteriophage that is specific to *S. arlettae* (i.e., *Staphylococcus arlettae*) on the surface of IRMOF-3. Combining the specificity of bacteriophages with the fluorescent nature of IRMOF-3, this biosensor exhibits excellent performance in detecting the *S. arlettae*. Moreover, there is a linear relationship between the logarithm of photoluminescence intensity and the logarithm of concentration of *S. arlettae* in the range of 10^2–10^8 cfu mL^{-1}. The practicability of bacteriophage/IRMOF-3 has also been verified because of the nearly consistent results obtained by using an optosensor and the colony counting method.[134] The variation of the specific bacteriophages makes it attractive to use IRMOF to fabricate selective and sensitive sensors for determining different bacteria.

Besides sensors that are based on the luminescence quenching effect, luminescence turn-on sensors have been fabricated by using IRMOF-3. The absorbance of IRMOF-3 is improved with the presence of M^{3+} ions (Cr^{3+}, Al^{3+}, Ga^{3+}, In^{3+}) and consequently the luminescent intensity is increased. According to Wang et al., this absorbance-caused enhancement (ACE) mechanism can be used to explain the potential of IRMOF-3 in detecting M^{3+} (Figure 20). The advantage of luminescence turn-on sensors is that they can be used with complex interference and this makes them more practical. The luminescence turn-on effect is not obvious when the M^{2+} ions (like Pb^{2+}, Cd^{2+}, and Cu^{2+}) and M^+ ions (such as Na^+ and Ag^+) are added. This result proves the selectivity of IRMOF-3 as a luminescence turn-on sensor for M^{3+} metal ions.[135]

2.3.3. IRMOF-8: Carbonization of Porous IRMOF-8 to Fabricate Electrochemical Sensors. Carbonization of IRMOF-8 can be achieved by different approaches. The various carbon materials are important components of sensors applied in environmental protection and healthcare. Porous carbon (abbreviated as PC) can be obtained from direct carbonization of IRMOF-8, and PC/GCE has been prepared

DOI: 10.1021/acs.cgd.9b00879
Cryst. Growth Des. 2019, 19, 7439−7462

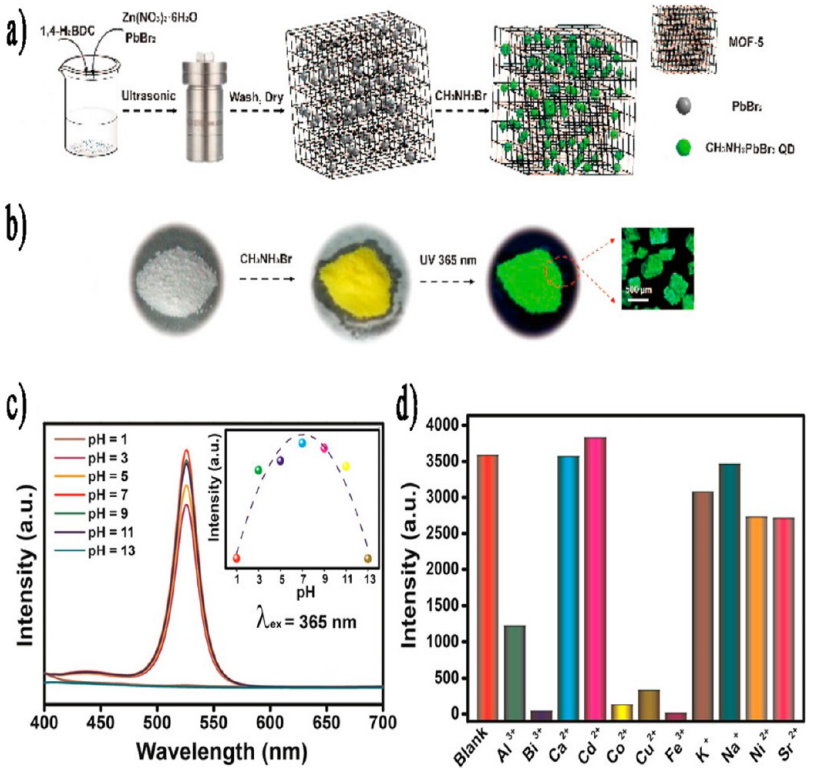

Figure 17. (a) Illustration of synthesis of $CH_3NH_3PbBr_3$@MOF-5; (b) images of fluorescence that $CH_3NH_3PbBr_3$@MOF-5 shows under UV light at wavelength of 365 nm and microscope morphology of this fluorescent composite; (c) effect of pH on photoluminescence spectra of $CH_3NH_3PbBr_3$@MOF-5 and peak emission intensities (inset); (d) selective luminescent responses to 11 metal ions of $CH_3NH_3PbBr_3$@MOF-5. (Reproduced from ref 129.)

by dropping the PC dispersion onto the surface of GCE. Subsequently, a voltammetric sensor has been obtained by fabricating molecularly imprinted polymer (MIP) on PC/GCE (Figure 21a). The considerable surface area and pore volume of PC are helpful for electron transportation. Thus, the conductivity of the sensor has been enhanced. This MIP/PC/GCE sensor can be utilized in detecting ultratrace levels of lidocaine (LID), a drug that might cause disease.[136]

With the addition of dispersing IRMOF-8 in a ceramic boat before the direct carbonization, IRMOF-8 derived nanoporous carbon (NPC) has been prepared. Then, NPC−Nafion/Bi/GCE composite electrode, a sensor for Pb(II) ions, has been synthesized by comodifying GCE electrode with NPC, Nafion, and bismuth (Figure 21b,c). The selectivity of this sensor has been confirmed by its anti-interference performance for Co(II), Zn(II), and other heavy metal ions as shown in Figure 21d. Additionally, interference of Cu(II) can be suppressed with the use of ferrocyanide. Similar to the case of MIP/PC/GCE, the excellent electrical conductivity of NPC can help to improve the sensitivity of NPC−Nafion/Bi/GCE. The satisfactory performance of NPC−Nafion/Bi/GCE in real tap water also indicates the applications of IRMOF-8-based sensors in environmental protection.[137]

To transform IRMOF-8 derived nanoporous carbon (abbreviated as DPC) into exfoliated porous carbon (EPC), Xiao et al. have employed the method of solvent exfoliation that includes dispersion of DPC in appropriate solvent, sonicating the solution, and subsequent processes. The BET surface areas and N_2 adsorption−desorption curves of DPC and EPC are exhibited in Figure 21e. EPC/GCE has been fabricated in a simple drop-casting method that is also utilized in synthesis of PC/GCE. In comparison with DPC/GCE, EPC/GCE exhibits better performance in detecting chloramphenicol (abbreviated as CAP) (Figure 21f). The low LOD (2.9×10^{-9} mol L^{-1}) and linear range for CAP reflect the practicality of EPC/GCE (Figure 21g). Moreover, this electrochemical sensor also owns outstanding repeatability, reproducibility, and stability.[138]

3. CONCLUSIONS AND OUTLOOK

MOFs including IRMOFs have drawn much attention for their excellent properties and attractive applications. In this Review, we have summarized the synthesis and potential applications of IRMOFs-*n* (*n* = 1, 3, 6, 8) in adsorption, separation, catalysis, and sensing.

Large surface areas and high pore volumes of IRMOFs-*n* (*n* = 1, 3, 6, 8) imply that they can act as high-performance sorbents. The published results of adsorption experiments of several small gases such as H_2, CO_2, N_2, and CH_4 in IRMOFs-*n* (*n* = 1, 3, 6, 8) show that pure IRMOF-1 is an outstanding adsorbent of CO_2 while pristine IRMOF-6 and IRMOF-8 are both candidates for H_2 storage. The pristine IRMOFs can also be adsorbents of gaseous contaminants. For example, IRMOF-3 with NH_2-containing linkers can be used to remove ammonia and chlorine. The selective adsorption is another highlight of IRMOFs. Specifically, IRMOF-3 adsorbs CO_2 over N_2 and IRMOF-8 can adsorb ethane from ethylene selectively. IRMOF-6 is also able to separate the alkene isomer mixture. It is desirable that the adsorption performance of IRMOFs can be improved in various ways. The use of spillover is an effective way to make IRMOF-1 and IRMOF-8 more ideal for hydrogen storage. IRMOF-3 derived N-doped carbon monolith shows

DOI: 10.1021/acs.cgd.9b00879
Cryst. Growth Des. 2019, 19, 7439−7462

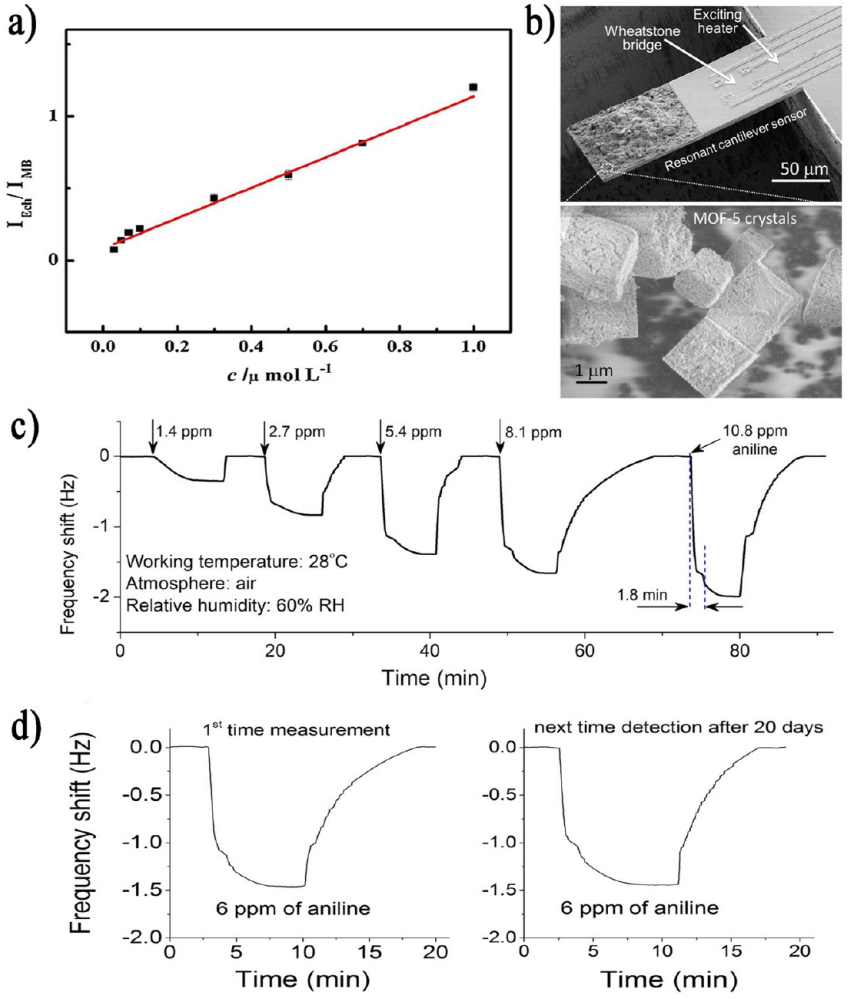

Figure 18. Applications of IRMOF-1 on electrochemical sensing and microgravimetric sensing. (a) Linear relationship between concentration of echinacoside and the ratio of electrochemical signal of echinacoside and peak current of methylene blue (I_{Ech}/I_{MB}); (b) SEM image of MOF-5 based microgravimetric sensor and MOF-5 serve as sensing materials; (c) response of microgravimetric sensor to aniline vapor with different concentrations; (d) long-term stability of MOF-5 based microgravimetric sensor. (a: Reproduced with permission from ref 130. Copyright Elsevier, 2018. b–d: Reproduced with permission from ref 131. Copyright Elsevier, 2018.)

enhanced selective adsorption of CO_2 from N_2, and IRMOF-3-Ag-*n* are remarkable capturers of DBT.

IRMOFs are emerging materials for catalyzing various reactions. We have focused on applications of IRMOF-1 in photocatalysis and catalyzing Friedel–Crafts alkylation in this Review. The BiOBr/MOF-5(IL) composite and HOQ@MOF-5 prove to be photocatalysts for degradation of methyl orange and phenyl, respectively. Two high-performance catalysts for Friedel–Crafts alkylation have been fabricated by hybridizing IRMOF-1 with attapulgite and SBA-15, respectively. We have also introduced the employment of IRMOF-3 as catalysts. Many approaches have been put forward to transform this IRMOF into outstanding catalysts, for instance, (1) single step and multistep postsynthetic modification of IRMOF-3; (2) utilization of IRMOF-3 derived nanocarbon materials; (3) synthesis of IRMOF-3 membrane in substrate; (4) preparation of core–shell IRMOF-3 composite.

IRMOFs and their derivatives can also act as keen sensors and detectors. The luminescence nature of IRMOF-1 and IRMOF-3 has been well-studied and utilized in the detection of isobutanol, glucose, and some heavy metal ions including Fe(III) and Cu(II). Metal ions (Cr^{3+}, Al^{3+}, Ga^{3+}, In^{3+}) can be detected by luminescence turn-on sensor based on IRMOF-3 because of the absorbance caused enhancement (ACE) mechanism. Additionally, it is a new developing trend to make use of IRMOFs in electrochemical and microgravimetric sensing. MB encased MOF-5@PGN/GCE sensor for echinacoside and IRMOF-1 loaded microcantilever sensor for aniline are good examples in this field. The effective detection of *S. arlettae* also signifies the potential of IRMOFs in biorecognition. Unlike IRMOF-1 and IRMOF-3, IRMOF-8 plays a role of sensor in the form of its derived carbon materials. Sensors for LID, Pb(II) ions, and CAP have been fabricated by combining these carbon materials and other components including GCE.

As introduced in this Review, many advances have been made in the synthesis, modification, functionalization, and application of IRMOFs. However, there remain some barriers in employing IRMOFs-*n* (n = 1, 3, 6, 8) and other IRMOFs in fields like energy industry and environmental protection: (1) lack of synthetic strategy that is handy, economic enough, and universal for IRMOFs; (2) the methods to enhance the hydrostability of IRMOFs might need some improvements because the instability in moisture limits the applications of some IRMOFs (such as IRMOF-1 and IRMOF-3); (3) IRMOFs and their derivatives show properties (such as

DOI: 10.1021/acs.cgd.9b00879
Cryst. Growth Des. 2019, 19, 7439–7462

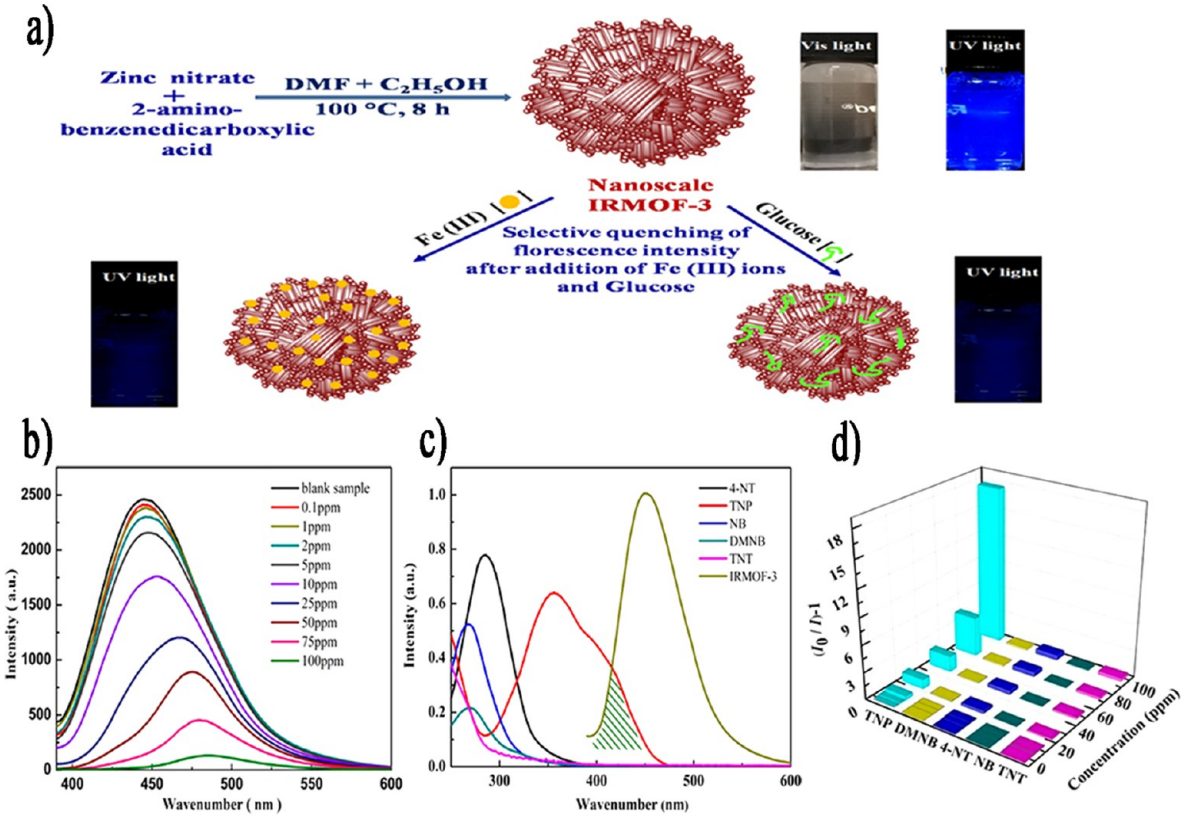

Figure 19. Applications of nanoscale IRMOF-3 on detecting (a) hydrothermal synthesis of nanoscale IRMOF-3 and its applications in detecting glucose and Fe^{3+} ions; (b) fluorescence emission spectra of IRMOF-3 with different concentrations of TNP; (c) comparison of emission spectrum of IRMOF-3 and absorbance spectrum of TNP and other kinds of nitro explosives, and (d) Stern−Volmer histogram for 2,4,6-trinitrophenol (TNP) and other analytes. (a: Reproduced with permission from ref 132. Copyright Elsevier, 2018. b,c,d: Reproduced from ref 133.).

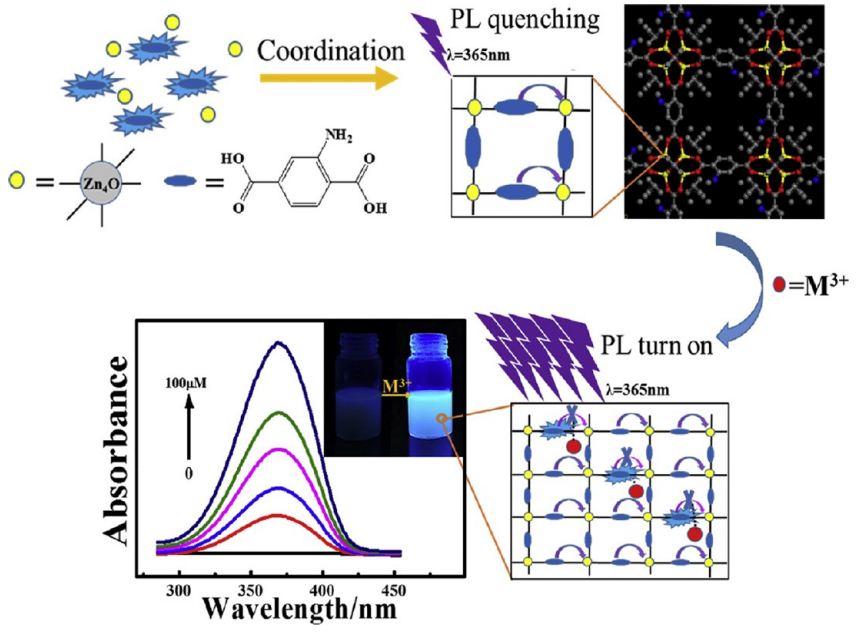

Figure 20. Schematic diagram of ACE mechanism of employing IRMOF-3 as a luminescence turn-on sensor for M^{3+}. (Reproduced with permission from ref 135. Copyright Elsevier, 2018.)

hydrogen storage capacity) that are more outstanding than some other MOFs but not up to the standard of the industry. The current experiments in applications of IRMOFs-*n* (*n* = 1, 3, 6, 8) provide some inspiration for future work. For instance, preparing IRMOFs in small size might endow these crystals with fascinating characteristics like improved catalytic activity. As known to us all, the use of natural materials in fabricating hybrid materials is not only more economic but also more environmentally friendly. The successful trial in preparing hybrid material of IRMOF-1 and attapulgite shows promising

DOI: 10.1021/acs.cgd.9b00879
Cryst. Growth Des. 2019, 19, 7439−7462

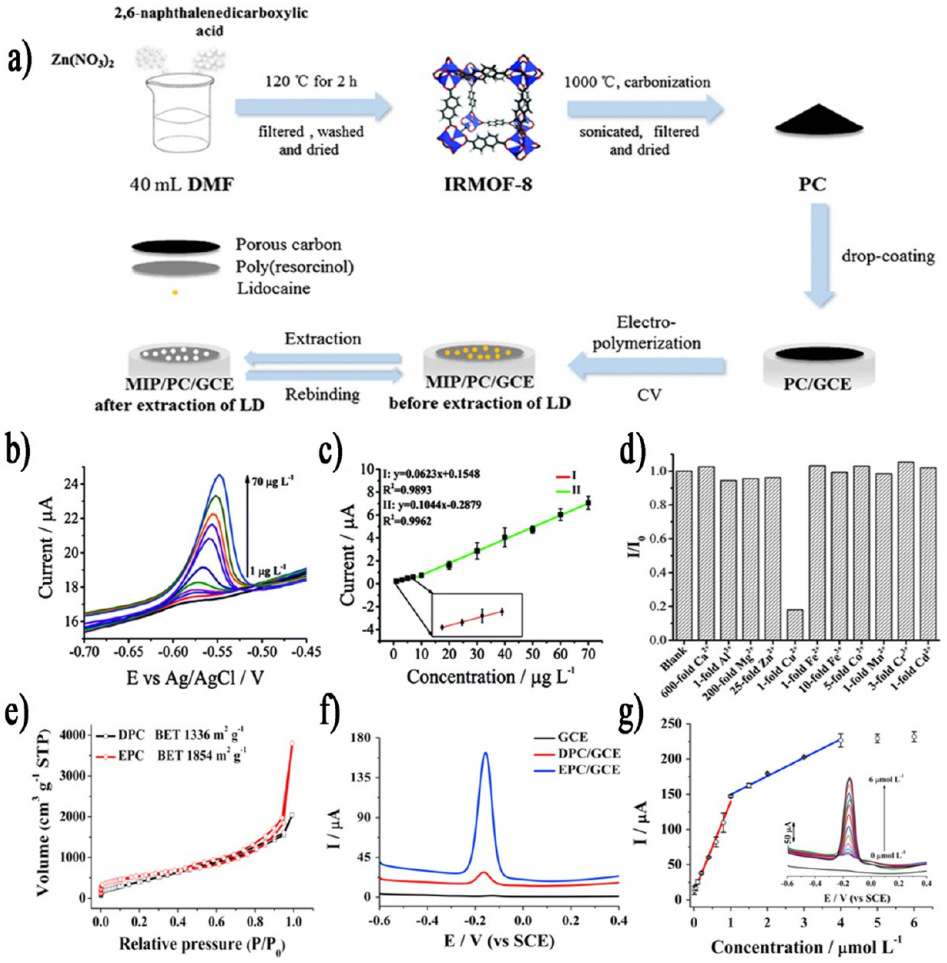

Figure 21. IRMOF-8 derived carbon materials are utilized to fabricate sensors. (a) Fabrication of MIP/PC/GCE; (b) differential pulse anodic stripping voltammetry curves that exhibit the performance of NPC−Nafion/Bi/GCE in detecting a concentration range of Pb(II); (c) linear relationship between stripping peak currents and concentration of Pb(II); (d) ratio of stripping current before (I_0) and after (I) the addition of different cations as interference; (e) BET surface areas and N_2 adsorption−desorption curves of DPC and EPC; (f) comparison of SWV curves of three electrodes with CAP concentration of 1×10^{-6} mol L^{-1}; (g) linear relationship between peak currents and concentration of CAP (inset: square wave voltammetry (SWV) curves when the concentrations of CAP are changed). (a: Reproduced with permission from ref 136. Copyright Springer Nature, 2017. b, c, and d: Reproduced with permission from ref 137. Copyright Royal Society of Chemistry, 2015. e, f and g: Reproduced with permission from ref 138. Copyright Elsevier, 2017.)

prospect to fabricate composites by utilizing IRMOFs and other natural materials.

AUTHOR INFORMATION

Corresponding Author

*E-mail: liudx9@mail.sysu.edu.cn (Dingxin Liu).

ORCID

Dingxin Liu: 0000-0002-8021-752X

Notes

The authors declare no competing financial interest.

ACKNOWLEDGMENTS

This work was supported by the National Natural Science Foundation of China (Grant No. 51603052) and the Fundamental Research Funds for the Central Universities (Grant No. 18lgpy02).

REFERENCES

(1) Chung, Y. G.; Camp, J.; Haranczyk, M.; Sikora, B. J.; Bury, W.; Krungleviciute, V.; Yildirim, T.; Farha, O. K.; Sholl, D. S.; Snurr, R. Q. Computation-Ready, Experimental Metal−Organic Frameworks: A Tool To Enable High-Throughput Screening of Nanoporous Crystals. *Chem. Mater.* **2014**, *26* (21), 6185−6192.

(2) Jiang, P.; Hu, Y.; Li, G. Biocompatible Au@Ag nanorod@ZIF-8 core-shell nanoparticles for surface-enhanced Raman scattering imaging and drug delivery. *Talanta* **2019**, *200*, 212−217.

(3) Mahmoodi, N. M.; Taghizadeh, M.; Taghizadeh, A.; Abdi, J.; Hayati, B.; Shekarchi, A. A. Bio-based magnetic metal-organic framework nanocomposite: Ultrasound-assisted synthesis and pollutant (heavy metal and dye) removal from aqueous media. *Appl. Surf. Sci.* **2019**, *480*, 288−299.

(4) Rasheed, H. U.; Lv, X.; Zhang, S.; Wei, W.; Ullah, N.; Xie, J. Ternary MIL-100(Fe)@Fe3O4/CA magnetic nanophotocatalysts (MNPCs): Magnetically separable and Fenton-like degradation of tetracycline hydrochloride. *Adv. Powder Technol.* **2018**, *29* (12), 3305−3314.

(5) Hu, T.; Jia, Q.; He, S.; Shan, S.; Su, H.; Zhi, Y.; He, L. Novel functionalized metal-organic framework MIL-101 adsorbent for capturing oxytetracycline. *J. Alloys Compd.* **2017**, *727*, 114−122.

(6) Yin, H. Q.; Yang, J. C.; Yin, X. B. Ratiometric Fluorescence Sensing and Real-Time Detection of Water in Organic Solvents with One-Pot Synthesis of Ru@MIL-101(Al)-NH2. *Anal. Chem.* **2017**, *89* (24), 13434−13440.

DOI: 10.1021/acs.cgd.9b00879
Cryst. Growth Des. 2019, 19, 7439−7462

(7) Zhao, Z.; Wang, S.; Yang, Y.; Li, X.; Li, J.; Li, Z. Competitive adsorption and selectivity of benzene and water vapor on the microporous metal organic frameworks (HKUST-1). *Chem. Eng. J.* **2015**, *259*, 79−89.
(8) Bae, J.; Jung, J. W.; Park, H. Y.; Cho, C. H.; Park, J. Oxygen plasma treatment of HKUST-1 for porosity retention upon exposure to moisture. *Chem. Commun.* **2017**, *53* (89), 12100−12103.
(9) Mazaj, M.; Čendak, T.; Buscarino, G.; Todaro, M.; Zabukovec Logar, N. Confined crystallization of a HKUST-1 metal−organic framework within mesostructured silica with enhanced structural resistance towards water. *J. Mater. Chem. A* **2017**, *5* (42), 22305−22315.
(10) Chen, Y.; Li, P.; Noh, H.; Kung, C. W.; Buru, C. T.; Wang, X.; Zhang, X.; Farha, O. K. Stabilization of Formate Dehydrogenase in a Metal-Organic Frame-work for Bioelectrocatalytic Reduction of CO(2). *Angew. Chem.* **2019**, *131*, 7764.
(11) Lyu, J.; Zhang, X.; Otake, K. I.; Wang, X.; Li, P.; Li, Z.; Chen, Z.; Zhang, Y.; Wasson, M. C.; Yang, Y.; Bai, P.; Guo, X.; Islamoglu, T.; Farha, O. K. Topology and porosity control of metal-organic frameworks through linker functionalization. *Chem. Sci.* **2019**, *10* (4), 1186−1192.
(12) Zhang, W.; Ma, Y.; Santos-Lopez, I. A.; Lownsbury, J. M.; Yu, H.; Liu, W. G.; Truhlar, D. G.; Campbell, C. T.; Vilches, O. E. Energetics of van der Waals Adsorption on the Metal-Organic Framework NU-1000 with Zr6-oxo, Hydroxo, and Aqua Nodes. *J. Am. Chem. Soc.* **2018**, *140* (1), 328−338.
(13) Tavares, S. R.; Ramsahye, N.; Maurin, G.; Leitão, A. A. Computational exploration of the structure, stability and adsorption properties of the ZIF-9 metal-organic framework. *Microporous Mesoporous Mater.* **2017**, *254*, 170−177.
(14) Pal, A.; Chand, S.; Elahi, S. M.; Das, M. C. A microporous MOF with a polar pore surface exhibiting excellent selective adsorption of CO_2 from CO_2-N_2 and CO_2-CH_4 gas mixtures with high CO_2 loading. *Dalton Trans* **2017**, *46* (44), 15280−15286.
(15) Niu, Z.; Guan, Q.; Shi, Y.; Chen, Y.; Chen, Q.; Kong, Z.; Ning, P.; Tian, S.; Miao, R. A lithium-modified zirconium-based metal organic framework (UiO-66) for efficient CO_2 adsorption. *New J. Chem.* **2018**, *42* (24), 19764−19770.
(16) Daliran, S.; Santiago-Portillo, A.; Navalon, S.; Oveisi, A. R.; Alvaro, M.; Ghorbani-Vaghei, R.; Azarifar, D.; Garcia, H. Cu(II)-Schiff base covalently anchored to MIL-125(Ti)-NH_2 as heterogeneous catalyst for oxidation reactions. *J. Colloid Interface Sci.* **2018**, *532*, 700−710.
(17) Baek, J.; Rungtaweevoranit, B.; Pei, X.; Park, M.; Fakra, S. C.; Liu, Y. S.; Matheu, R.; Alshmimri, S. A.; Alshehri, S.; Trickett, C. A.; Somorjai, G. A.; Yaghi, O. M. Bioinspired Metal-Organic Framework Catalysts for Selective Methane Oxidation to Methanol. *J. Am. Chem. Soc.* **2018**, *140* (51), 18208−18216.
(18) Fu, G.; Bueken, B.; De Vos, D. Zr-Metal-Organic Framework Catalysts for Oxidative Desulfurization and Their Improvement by Postsynthetic Ligand Exchange. *Small Methods* **2018**, *2* (12), 1800059.
(19) He, H.; Xue, Y. Q.; Wang, S. Q.; Zhu, Q. Q.; Chen, J.; Li, C. P.; Du, M. A Double-Walled Bimetal-Organic Framework for Antibiotics Sensing and Size-Selective Catalysis. *Inorg. Chem.* **2018**, *57* (24), 15062−15068.
(20) Sk, M.; Banesh, S.; Trivedi, V.; Biswas, S. Selective and Sensitive Sensing of Hydrogen Peroxide by a Boronic Acid Functionalized Metal-Organic Framework and Its Application in Live-Cell Imaging. *Inorg. Chem.* **2018**, *57* (23), 14574−14581.
(21) Liu, L.; Wang, Y.; Lin, R.; Yao, Z.; Lin, Q.; Wang, L.; Zhang, Z.; Xiang, S. Two water-stable lanthanide metal-organic frameworks with oxygen-rich channels for fluorescence sensing of Fe(iii) ions in aqueous solution. *Dalton Trans* **2018**, *47* (45), 16190−16196.
(22) Zhong, X.; Zhang, Y.; Tan, L.; Zheng, T.; Hou, Y.; Hong, X.; Du, G.; Chen, X.; Zhang, Y.; Sun, X. An aluminum adjuvant-integrated nano-MOF as antigen delivery system to induce strong humoral and cellular immune responses. *J. Controlled Release* **2019**, *300*, 81−92.
(23) Nejadshafiee, V.; Naeimi, H.; Goliaei, B.; Bigdeli, B.; Sadighi, A.; Dehghani, S.; Lotfabadi, A.; Hosseini, M.; Nezamtaheri, M. S.; Amanlou, M.; Sharifzadeh, M.; Khoobi, M. Magnetic bio-metal-organic framework nanocomposites decorated with folic acid conjugated chitosan as a promising biocompatible targeted theranostic system for cancer treatment. *Mater. Sci. Eng., C* **2019**, *99*, 805−815.
(24) Ma, D.; Xie, J.; Zhu, Z.; Huang, H.; Chen, Y.; Su, R.; Zhu, H. Drug delivery and selective CO_2 adsorption of a bio-based porous zinc-organic framework from 2,5-furandicarboxylate ligand. *Inorg. Chem. Commun.* **2017**, *19* (35), 5244−5250.
(25) Eddaoudi, M. K.; Jaheon; Rosi, N.; Vodak, D.; Wachter, J. O. K.; Michael; Yaghi, O. M. Systematic design of pore size and functionality in isoreticular MOFs and their application in methane storage. *Science* **2002**, *295*, 469.
(26) Britt, D.; Tranchemontagne, D.; Yaghi, O. M. Metal-organic frameworks with high capacity and selectivity for harmful gases. *Proc. Natl. Acad. Sci. U. S. A.* **2008**, *105* (33), 11623−11627.
(27) Millward, A. R.; Yaghi, O. M. Metal-Organic Frameworks with Exceptionally High Capacity for Storage of Carbon Dioxide at Room Temperature. *J. Am. Chem. Soc.* **2005**, *127*, 17998.
(28) Rowsell, J. L. C.; Yaghi, O. M. Effects of Functionalization, Catenation, and Variation of the Metal Oxide and Organic Linking Units on the Low-Pressure Hydrogen Adsorption Properties of Metal-Organic Frameworks. *J. Am. Chem. Soc.* **2006**, *128* (4), 1304−1315.
(29) Li, Y.; Yang, R. T. Significantly Enhanced Hydrogen Storage in Metal-Organic Frameworks via Spillover. *J. Am. Chem. Soc.* **2006**, *128*, 726−727.
(30) Rowsell, J. L. C.; Millward, A. R.; Park, K. S.; Yaghi, O. M. Hydrogen Sorption in Functionalized Metal-Organic Frameworks. *J. Am. Chem. Soc.* **2004**, *126*, 5666.
(31) Gutov, O. V.; Bury, W.; Gomez-Gualdron, D. A.; Krungleviciute, V.; Fairen-Jimenez, D.; Mondloch, J. E.; Sarjeant, A. A.; Al-Juaid, S. S.; Snurr, R. Q.; Hupp, J. T.; Yildirim, T.; Farha, O. K. Water-Stable Zirconium-Based Metal−Organic Framework Material with High-Surface Area and Gas-Storage Capacities. *Chem. - Eur. J.* **2014**, *20*, 12389−12393.
(32) Borah, B.; Zhang, H.; Snurr, R. Q. Diffusion of methane and other alkanes in metal-organic frameworks for natural gas storage. *Chem. Eng. Sci.* **2015**, *124*, 135−143.
(33) Latroche, M.; Surblé, S.; Serre, C.; Mellot-Draznieks, C.; Llewellyn, P. L.; Lee, J.-H.; Chang, J.-S.; Jhung, S. H.; Férey, G. Hydrogen Storage in the Giant-Pore Metal−Organic Frameworks MIL-100 and MIL-101. *Angew. Chem., Int. Ed.* **2006**, *45* (48), 8227−8231.
(34) Rivera-Torrente, M.; Pletcher, P. D.; Jongkind, M. K.; Nikolopoulos, N.; Weckhuysen, B. M. Ethylene Polymerization over Metal−Organic Framework Crystallites and the Influence of Linkers on Their Fracturing Process. *ACS Catal.* **2019**, *9* (4), 3059−3069.
(35) Yang, H.; He, X.-W.; Wang, F.; Kang, Y.; Zhang, J. Doping copper into ZIF-67 for enhancing gas uptake capacity and visible-light-driven photocatalytic degradation of organic dye. *J. Mater. Chem.* **2012**, *22* (41), 21849.
(36) Khay, I.; Chaplais, G.; Nouali, H.; Ortiz, G.; Marichal, C.; Patarin, J. Assessment of the energetic performances of various ZIFs with SOD or RHO topology using high pressure water intrusion−extrusion experiments. *Dalton Trans* **2016**, *45* (10), 4392−4400.
(37) Park, K. S.; Ni, Z.; Cote, A. P.; Choi, J. Y.; Huang, R.; Uribe-Romo, F. J.; Chae, H. K.; O'Keeffe, M.; Yaghi, O. M. Exceptional chemical and thermal stability of zeolitic imidazolate frameworks. *Proc. Natl. Acad. Sci. U. S. A.* **2006**, *103* (27), 10186−10191.
(38) Jeong, N. C.; Samanta, B.; Lee, C. Y.; Farha, O. K.; Hupp, J. T. Coordination-chemistry control of proton conductivity in the iconic metal-organic framework material HKUST-1. *J. Am. Chem. Soc.* **2012**, *134* (1), 51−4.
(39) Parkes, M. V.; Staiger, C. L.; Perry, J. J.; Allendorf, M. D.; Greathouse, J. A. Screening metal−organic frameworks for selective noble gas adsorption in air: effect of pore size and framework topology. *Phys. Chem. Chem. Phys.* **2013**, *15* (23), 9093.

DOI: 10.1021/acs.cgd.9b00879
Cryst. Growth Des. 2019, 19, 7439−7462

(40) Li, C.; Qiu, W.; Shi, W.; Song, H.; Bai, G.; He, H.; Li, J.; Zaworotko, M. J. A pcu-type metal−organic framework based on covalently quadruple cross-linked supramolecular building blocks (SBBs): structure and adsorption properties. *CrystEngComm* **2012**, *14* (6), 1929.
(41) Bhunia, A.; Dey, S.; Moreno, J. M.; Diaz, U.; Concepcion, P.; Van Hecke, K.; Janiak, C.; Van Der Voort, P. A homochiral vanadium-salen based cadmium bpdc MOF with permanent porosity as an asymmetric catalyst in solvent-free cyanosilylation. *Chem. Commun.* **2016**, *52* (7), 1401−4.
(42) He, H.; Song, Y.; Sun, F.; Bian, Z.; Gao, L.; Zhu, G. A porous metal−organic framework formed by a V-shaped ligand and Zn(ii) ion with highly selective sensing for nitroaromatic explosives. *J. Mater. Chem. A* **2015**, *3* (32), 16598−16603.
(43) Sun, X.; Yao, S.; Yu, C.; Li, G.; Liu, C.; Huo, Q.; Liu, Y. An ultrastable Zr-MOF for fast capture and highly luminescence detection of $Cr_2O_7^{2-}$ simultaneously in an aqueous phase. *J. Mater. Chem. A* **2018**, *6* (15), 6363−6369.
(44) Son, W. J.; Kim, J.; Kim, J.; Ahn, W. S. Sonochemical synthesis of MOF-5. *Chem. Commun.* **2008**, No. 47, 6336−8.
(45) Firth, F. C. N.; Cliffe, M. J.; Vulpe, D.; Aragones-Anglada, M.; Moghadam, P. Z.; Fairen-Jimenez, D.; Slater, B.; Grey, C. P. Engineering new defective phases of UiO family metal−organic frameworks with water. *J. Mater. Chem. A* **2019**, *7* (13), 7459−7469.
(46) Liu, L.; Chen, Z.; Wang, J.; Zhang, D.; Zhu, Y.; Ling, S.; Huang, K.-W.; Belmabkhout, Y.; Adil, K.; Zhang, Y.; Slater, B.; Eddaoudi, M.; Han, Y. Imaging defects and their evolution in a metal−organic framework at sub-unit-cell resolution. *Nat. Chem.* **2019**, *11* (7), 622−628.
(47) Yuan, L.; Tian, M.; Lan, J.; Cao, X.; Wang, X.; Chai, Z.; Gibson, J. K.; Shi, W. Defect engineering in metal−organic frameworks: a new strategy to develop applicable actinide sorbents. *Chem. Commun.* **2018**, *54* (4), 370−373.
(48) Park, T. H.; Hickman, A. J.; Koh, K.; Martin, S.; Wong-Foy, A. G.; Sanford, M. S.; Matzger, A. J. Highly dispersed palladium(II) in a defective metal-organic framework: application to C-H activation and functionalization. *J. Am. Chem. Soc.* **2011**, *133* (50), 20138−41.
(49) Sarkisov, L. Molecular simulation of low temperature argon adsorption in several models of IRMOF-1 with defects and structural disorder. *Dalton Trans* **2016**, *45* (10), 4203−12.
(50) Faustini, M.; Kim, J.; Jeong, G. Y.; Kim, J. Y.; Moon, H. R.; Ahn, W. S.; Kim, D. P. Microfluidic approach toward continuous and ultrafast synthesis of metal-organic framework crystals and hetero structures in confined microdroplets. *J. Am. Chem. Soc.* **2013**, *135* (39), 14619−26.
(51) Zhao, J.; Nunn, W. T.; Lemaire, P. C.; Lin, Y.; Dickey, M. D.; Oldham, C. J.; Walls, H. J.; Peterson, G. W.; Losego, M. D.; Parsons, G. N. Facile Conversion of Hydroxy Double Salts to Metal-Organic Frameworks Using Metal Oxide Particles and Atomic Layer Deposition Thin-Film Templates. *J. Am. Chem. Soc.* **2015**, *137* (43), 13756−9.
(52) Yang, H.-m.; Liu, X.; Song, X.-l.; Yang, T.-l.; Liang, Z.-h.; Fan, C.-m. In situ electrochemical synthesis of MOF-5 and its application in improving photocatalytic activity of BiOBr. *Trans. Nonferrous Met. Soc. China* **2015**, *25*, 3987.
(53) Li, J. R.; Sculley, J.; Zhou, H. C. Metal-organic frameworks for separations. *Chem. Rev.* **2012**, *112* (2), 869−932.
(54) Cychosz, K. A.; Matzger, A. J. Water Stability of Microporous Coordination Polymers and the Adsorption of Pharmaceuticals from Water. *Langmuir* **2010**, *26* (22), 17198−17202.
(55) Mason, J. A.; Veenstra, M.; Long, J. R. Evaluating metal−organic frameworks for natural gas storage. *Chem. Sci.* **2014**, *5* (1), 32−51.
(56) Feldblyum, J. I.; Dutta, D.; Wong-Foy, A. G.; Dailly, A.; Imirzian, J.; Gidley, D. W.; Matzger, A. J. Interpenetration, Porosity, and High-Pressure Gas Adsorption in Zn_4O(2,6-naphthalene dicarboxylate)3. *Langmuir* **2013**, *29* (25), 8146−8153.
(57) Llewellyn, P. L.; Bourrelly, S. S.; Christian; Vimont, A. D.; Marco; Hamon, L.; Weireld, G. D.; Chang, J.-S.; Hong, D.-Y.; Hwang, Y. K. J.; Sung Hwa; Férey, G. r. High Uptakes of CO_2 and CH_4 in Mesoporous Metal-Organic Frameworks MIL-100 and MIL-101. *Langmuir* **2008**, *24*, 7245−7250.
(58) Hong, D.-Y.; Hwang, Y. K.; Serre, C.; Férey, G.; Chang, J.-S. Porous Chromium Terephthalate MIL-101 with Coordinatively Unsaturated Sites: Surface Functionalization, Encapsulation, Sorption and Catalysis. *Adv. Funct. Mater.* **2009**, *19* (10), 1537−1552.
(59) Panchariya, D. K.; Rai, R. K.; Anil Kumar, E.; Singh, S. K. Core−Shell Zeolitic Imidazolate Frameworks for Enhanced Hydrogen Storage. *ACS Omega* **2018**, *3* (1), 167−175.
(60) Zhong, G.; Liu, D.; Zhang, J. The application of ZIF-67 and its derivatives: adsorption, separation, electrochemistry and catalysts. *J. Mater. Chem. A* **2018**, *6* (5), 1887−1899.
(61) Awadallah-F, A.; Hillman, F.; Al-Muhtaseb, S. A.; Jeong, H.-K. Adsorption Equilibrium and Kinetics of Nitrogen, Methane and Carbon Dioxide Gases onto ZIF-8, Cu10%/ZIF-8, and Cu30%/ZIF-8. *Ind. Eng. Chem. Res.* **2019**, *58* (16), 6653−6661.
(62) Al-Naddaf, Q.; Al-Mansour, M.; Thakkar, H.; Rezaei, F. MOF-GO Hybrid Nanocomposite Adsorbents for Methane Storage. *Ind. Eng. Chem. Res.* **2018**, *57* (51), 17470−17479.
(63) Cortés-Súarez, J.; Celis-Arias, V.; Beltrán, H. I.; Tejeda-Cruz, A.; Ibarra, I. A.; Romero-Ibarra, J. E.; Sánchez-González, E.; Loera-Serna, S. Synthesis and Characterization of an SWCNT@HKUST-1 Composite: Enhancing the CO_2 Adsorption Properties of HKUST-1. *ACS Omega* **2019**, *4* (3), 5275−5282.
(64) Xiao, B.; Wheatley, P. S.; Zhao, X.; Fletcher, A. J.; Fox, S.; Rossi, A. G.; Megson, I. L.; Bordiga, S.; Regli, L.; Thomas, K. M.; Morris, R. E. High-Capacity Hydrogen and Nitric Oxide Adsorption and Storage in a Metal-Organic Framework. *J. Am. Chem. Soc.* **2007**, *129*, 1203−1209.
(65) Zhang, H.; Deria, P.; Farha, O. K.; Hupp, J. T.; Snurr, R. Q. A thermodynamic tank model for studying the effect of higher hydrocarbons on natural gas storage in metal−organic frameworks. *Energy Environ. Sci.* **2015**, *8*, 1501.
(66) Ding, S.; Dong, Q.; Hu, J.; Xiao, W.; Liu, X.; Liao, L.; Zhang, N. Enhanced selective adsorption of CO_2 on nitrogen-doped porous carbon monoliths derived from IRMOF-3. *Chem. Commun.* **2016**, *52* (63), 9757−9760.
(67) Zhang, L.; Wang, Q.; Wu, T.; Liu, Y. C. Understanding adsorption and interactions of alkane isomer mixtures in isoreticular metal-organic frameworks. *Chem. - Eur. J.* **2007**, *13* (22), 6387−96.
(68) Rosi, N. L.; Eckert, J. E.; Mohamed, V.; David, T.; Kim, J.; O'Keeffe, M.; Yaghi, O. M. Hydrogen Storage in Microporous Metal-Organic Frameworks. *Science* **2003**, *300*, 1127.
(69) Li, D.; Wang, H.; Zhang, X.; Sun, H.; Dai, X.; Yang, Y.; Ran, L.; Li, X.; Ma, X.; Gao, D. Morphology Design of IRMOF-3 Crystal by Coordination Modulation. *Cryst. Growth Des.* **2014**, *14* (11), 5856−5864.
(70) Li, Y.; Yang, R. T. Hydrogen Storage in Metal-Organic Frameworks by Bridged Hydrogen Spillover. *J. Am. Chem. Soc.* **2006**, *128*, 8136.
(71) Pires, J.; Pinto, M. L.; Saini, V. K. Ethane Selective IRMOF-8 and Its Significance in Ethane−Ethylene Separation by Adsorption. *ACS Appl. Mater. Interfaces* **2014**, *6* (15), 12093−12099.
(72) Siberio-Pérez, D. Y.; Wong-Foy, A. G.; Yaghi, O. M.; Matzger, A. J. Raman Spectroscopic Investigation of CH4and N2Adsorption in Metal-Organic Frameworks. *Chem. Mater.* **2007**, *19* (15), 3681−3685.
(73) Sreenivasulu, B.; Sreedhar, I.; Suresh, P.; Raghavan, K. V. Development Trends in Porous Adsorbents for Carbon Capture. *Environ. Sci. Technol.* **2015**, *49* (21), 12641−12661.
(74) Zhang, H.; Deria, P.; Farha, O. K.; Hupp, J. T.; Snurr, R. Q. A thermodynamic tank model for studying the effect of higher hydrocarbons on natural gas storage in metal−organic frameworks. *Energy Environ. Sci.* **2015**, *8* (5), 1501−1510.
(75) Ganz, E.; Dornfeld, M. Storage Capacity of Metal−Organic and Covalent−Organic Frameworks by Hydrogen Spillover. *J. Phys. Chem. C* **2012**, *116* (5), 3661−3666.
(76) Kou, J.; Sun, L.-B. Fabrication of Metal−Organic Frameworks inside Silica Nanopores with Significantly Enhanced Hydrostability

DOI: 10.1021/acs.cgd.9b00879
Cryst. Growth Des. 2019, 19, 7439−7462

and Catalytic Activity. *ACS Appl. Mater. Interfaces* **2018**, *10* (14), 12051−12059.
(77) Lu, L.; Li, X.-Y.; Liu, X.-Q.; Wang, Z.-M.; Sun, L.-B. Enhancing the hydrostability and catalytic performance of metal−organic frameworks by hybridizing with attapulgite, a natural clay. *J. Mater. Chem. A* **2015**, *3*, 6998−7005.
(78) Xu, S.; Lv, Y.; Zeng, X.; Cao, D. ZIF-derived nitrogen-doped porous carbons as highly efficient adsorbents for removal of organic compounds from wastewater. *Chem. Eng. J.* **2017**, *323*, 502−511.
(79) Sarker, M.; Ahmed, I.; Jhung, S. H. Adsorptive removal of herbicides from water over nitrogen-doped carbon obtained from ionic liquid@ZIF-8. *Chem. Eng. J.* **2017**, *323*, 203−211.
(80) Abo El Naga, A. O.; Shaban, S. A.; El Kady, F. Y. A. Metal organic framework-derived nitrogen-doped nanoporous carbon as an efficient adsorbent for methyl orange removal from aqueous solution. *J. Taiwan Inst. Chem. Eng.* **2018**, *93*, 363−373.
(81) Orefuwa, S. A.; Yang, H.; Goudy, A. J. Rapid solvothermal synthesis of an isoreticular metal−organic framework with permanent porosity for hydrogen storage. *Microporous Mesoporous Mater.* **2012**, *153* (88−93), 88−93.
(82) Feldblyum, J. I.; Wong-Foy, A. G.; Matzger, A. J. Non-interpenetrated IRMOF-8: synthesis, activation, and gas sorption. *Chem. Commun.* **2012**, *48* (79), 9828−9830.
(83) Ardelean, O.; Blanita, G.; Borodi, G.; Mihet, M.; Coros, M.; Lupu, D. On the enhancement of hydrogen uptake by IRMOF-8 composites with Pt/carbon catalyst. *Int. J. Hydrogen Energy* **2012**, *37* (9), 7378−7384.
(84) Kuppler, R. J.; Timmons, D. J.; Fang, Q.-R.; Li, J.-R.; Makal, T. A.; Young, M. D.; Yuan, D.; Zhao, D.; Zhuang, W.; Zhou, H.-C. Potential applications of metal-organic frameworks. *Coord. Chem. Rev.* **2009**, *253* (23−24), 3042−3066.
(85) Lan, M.; Guo, R.-M.; Dou, Y.; Zhou, J.; Zhou, A.; Li, J.-R. Fabrication of porous Pt-doping heterojunctions by using bimetallic MOF template for photocatalytic hydrogen generation. *Nano Energy* **2017**, *33*, 238−246.
(86) Panda, A.; Kim, E.; Choi, Y.; Lee, J.; Venkateswarlu, S.; Yoon, M. Phase Controlled Synthesis of Pt Doped Co Nanoparticle Composites Using a Metal-Organic Framework for Fischer−Tropsch Catalysis. *Catalysts* **2019**, *9* (2), 156.
(87) Rostamnia, S.; Alamgholiloo, H.; Jafari, M. Ethylene diamine post-synthesis modification on open metal site Cr-MOF to access efficient bifunctional catalyst for the Hantzsch condensation reaction. *Appl. Organomet. Chem.* **2018**, *32* (8), e4370.
(88) Gascón, V.; Castro-Miguel, E.; Díaz-García, M.; Blanco, R. M.; Sanchez-Sanchez, M. In situ and post-synthesis immobilization of enzymes on nanocrystalline MOF platforms to yield active biocatalysts. *J. Chem. Technol. Biotechnol.* **2017**, *92* (10), 2583−2593.
(89) Cheng, S.; Shang, N.; Feng, C.; Gao, S.; Wang, C.; Wang, Z. Efficient multicomponent synthesis of propargylamines catalyzed by copper nanoparticles supported on metal-organic framework derived nanoporous carbon. *Catal. Commun.* **2017**, *89*, 91−95.
(90) Ning, L.; Liao, S.; Cui, H.; Yu, L.; Tong, X. Selective Conversion of Renewable Furfural with Ethanol to Produce Furan-2-acrolein Mediated by Pt@MOF-5. *ACS Sustainable Chem. Eng.* **2018**, *6* (1), 135−142.
(91) Guo, C.; Zhang, Y.; Zhang, L.; Zhang, Y.; Wang, J. 2-Methylimidazole-assisted synthesis of a two-dimensional MOF-5 catalyst with enhanced catalytic activity for the Knoevenagel condensation reaction. *CrystEngComm* **2018**, *20* (36), 5327−5331.
(92) Khan, I. A.; Qian, Y.; Badshah, A.; Nadeem, M. A.; Zhao, D. Highly Porous Carbon Derived from MOF-5 as a Support of ORR Electrocatalysts for Fuel Cells. *ACS Appl. Mater. Interfaces* **2016**, *8* (27), 17268−75.
(93) Thakare, S. R.; Ramteke, S. M. Postmodification of MOF-5 using secondary complex formation using 8- hydroxyquinoline (HOQ) for the development of visible light active photocatalysts. *J. Phys. Chem. Solids* **2018**, *116*, 264−272.
(94) Zhou, X.; Zhang, Y.; Yang, X.; Zhao, L.; Wang, G. Functionalized IRMOF-3 as efficient heterogeneous catalyst for the synthesis of cyclic carbonates. *J. Mol. Catal. A: Chem.* **2012**, *361-362*, 12.
(95) Maity, T.; Saha, D.; Das, S.; Bhunia, S.; Koner, S. Ligand free copper-catalyzed heterogeneous O-arylation reaction under green condition. *Catal. Commun.* **2015**, *58*, 141−148.
(96) Wang, G.; Chen, S.; Quan, X.; Yu, H.; Zhang, Y. Enhanced activation of peroxymonosulfate by nitrogen doped porous carbon for effective removal of organic pollutants. *Carbon* **2017**, *115*, 730−739.
(97) Lee, Y.-R.; Cho, S.-M.; Ahn, W.-S.; Lee, C.-H.; Lee, K.-H.; Cho, W.-S. Facile synthesis of an IRMOF-3 membrane on porous Al_2O_3 substrate via a sonochemical route. *Microporous Mesoporous Mater.* **2015**, *213*, 161−168.
(98) Li, W.; Li, G.; Liu, D. Synthesis and application of core−shell magnetic metal−organic framework composites Fe_3O_4/ IRMOF-3. *RSC Adv.* **2016**, *6*, 94113−94118.
(99) Zhang, Z.-H.; Zhang, J.-N.; Yang, X.-H.; Guo, W.-J.; Wang, B. Magnetic Metal−Organic Framework $CoFe_2O_4$@SiO_2@IRMOF-3 as an Efficient Catalyst for One-Pot Synthesis of Functionalized Dihydro-2-oxopyrroles. *Synlett* **2017**, *28* (06), 734−740.
(100) Gascon, J.; Hernμndez-Alonso, M. a. D.; Almeida, A. R.; Klink, G. P. M. v. K.; Freek; Mul, G. Isoreticular MOFs as Efficient Photocatalysts with Tunable Band Gap: An Operando FTIR Study of the Photoinduced Oxidation of Propylene. *ChemSusChem* **2008**, *1*, 981−983.
(101) Chatterjee, D.; Mahata, A. Photoassisted detoxi®cation of organic pollutants on the surface modi®ed TiO_2 semiconductor particulate system. *Catal. Commun.* **2001**, *2*, 1−3.
(102) Scott, T.; Zhao, H.; Deng, W.; Feng, X.; Li, Y. Photocatalytic degradation of phenol in water under simulated sunlight by an ultrathin MgO coated Ag/TiO_2 nanocomposite. *Chemosphere* **2019**, *216*, 1−8.
(103) Song, J.; Zhang, Z.; Hu, S.; Wu, T.; Jiang, T.; Han, B. MOF-5/n-Bu4NBr: an efficient catalyst system for the synthesis of cyclic carbonates from epoxides and CO_2 under mild conditions. *Green Chem.* **2009**, *11* (7), 1031−1036.
(104) Phan, N. T. S.; Le, K. K. A.; Phan, T. D. MOF-5 as an efficient heterogeneous catalyst for Friedel−Crafts alkylation reactions. *Appl. Catal., A* **2010**, *382* (2), 246−253.
(105) Li, Q.; Jiang, S.; Ji, S.; Shi, D.; Li, H. Synthesis of magnetically recyclable MOF-5@SiO_2@Fe_3O_4 catalysts and their catalytic performance of Friedel−Crafts alkylation. *J. Porous Mater.* **2015**, *22* (5), 1205−1214.
(106) Yuan, B.; Yin, X.-Q.; Liu, X.-Q.; Li, X.-Y.; Sun, L.-B. Enhanced Hydrothermal Stability and Catalytic Performance of HKUST-1 by Incorporating Carboxyl-Functionalized Attapulgite. *ACS Appl. Mater. Interfaces* **2016**, *8* (25), 16457−16464.
(107) Xie, X.-Y.; Qian, X.-Y.; Qi, S.-C.; Wu, J.-K.; Liu, X.-Q.; Sun, L.-B. Endowing Cu-BTC with Improved Hydrothermal Stability and Catalytic Activity: Hybridization with Natural Clay Attapulgite via Vapor-Induced Crystallization. *ACS Sustainable Chem. Eng.* **2018**, *6* (10), 13217−13225.
(108) Zhu, L.; Liu, X. Q.; Jiang, H. L.; Sun, L. B. Metal-Organic Frameworks for Heterogeneous Basic Catalysis. *Chem. Rev.* **2017**, *117* (12), 8129−8176.
(109) Sun, L.-B.; Liu, X.-Q.; Zhou, H.-C. Design and fabrication of mesoporous heterogeneous basic catalysts. *Chem. Soc. Rev.* **2015**, *44* (15), 5092−5147.
(110) Mei, S.; Gu, J.; Ma, T.; Li, X.; Hu, Y.; Li, W.; Zhang, J.; Han, Y. N-doped activated carbon from used dyeing wastewater adsorbent as a metal-free catalyst for acetylene hydrochlorination. *Chem. Eng. J.* **2019**, *371*, 118−129.
(111) Wu, K.; Chen, Z.; Cheong, W. C.; Liu, S.; Zhu, W.; Cao, X.; Sun, K.; Lin, Y.; Zheng, L.; Yan, W.; Pan, Y.; Wang, D.; Peng, Q.; Chen, C.; Li, Y. Toward Bifunctional Overall Water Splitting Electrocatalyst: General Preparation of Transition Metal Phosphide Nanoparticles Decorated N-Doped Porous Carbon Spheres. *ACS Appl. Mater. Interfaces* **2018**, *10* (51), 44201−44208.
(112) Wang, M. J.; Mao, Z. X.; Liu, L.; Peng, L.; Yang, N.; Deng, J.; Ding, W.; Li, J.; Wei, Z. Preparation of Hollow Nitrogen Doped

DOI: 10.1021/acs.cgd.9b00879
Cryst. Growth Des. 2019, 19, 7439−7462

Carbon via Stresses Induced Orientation Contraction. *Small* **2018**, *14* (52), No. e1804183.
(113) Wu, Y.-Q.; Xie, L.-H.; Qin, X.; Sun, Y.-X.; Xie, Y.-B.; Li, J.-R. Continuous Crystalline Membranes of a Ni(II)-Based Pillared-Layer Metal-Organic Framework In Situ Grown on Nickel Foam with Two Orientations. *Crystals* **2018**, *8* (10), 383.
(114) Denny, M. S., Jr.; Cohen, S. M. In Situ Modification of Metal-Organic Frameworks in Mixed-Matrix Membranes. *Angew. Chem., Int. Ed.* **2015**, *54* (31), 9029−32.
(115) Kong, C.; Du, H.; Chen, L.; Chen, B. Nanoscale MOF/organosilica membranes on tubular ceramic substrates for highly selective gas separation. *Energy Environ. Sci.* **2017**, *10* (8), 1812−1819.
(116) Liu, S.; Shinde, S.; Pan, J.; Ma, Y.; Yan, Y.; Pan, G. Interface-induced growth of boronate-based metal-organic framework membrane on porous carbon substrate for aqueous phase molecular recognition. *Chem. Eng. J.* **2017**, *324*, 216−227.
(117) Llabrés i Xamena, F. X.; Cirujano, F. G.; Corma, A. An unexpected bifunctional acid base catalysis in IRMOF-3 for Knoevenagel condensation reactions. *Microporous Mesoporous Mater.* **2012**, *157*, 112−117.
(118) Gascon, J.; Aktay, U.; Hernandezalonso, M.; Vanklink, G.; Kapteijn, F. Amino-based metal-organic frameworks as stable, highly active basic catalysts. *J. Catal.* **2009**, *261* (1), 75−87.
(119) Miao, Z.; Yang, F.; Luan, Y.; Shu, X.; Ramella, D. Synthesis of Fe_3O_4 @P4VP@ZIF-8 core-shell microspheres and their application in a Knoevenagel condensation reaction. *J. Solid State Chem.* **2017**, *256*, 27−32.
(120) Qi, M.-H.; Gao, M.-L.; Liu, L.; Han, Z.-B. Robust Bifunctional Core−Shell MOF@POP Catalyst for One-Pot Tandem Reaction. *Inorg. Chem.* **2018**, *57* (23), 14467−14470.
(121) Song, Z.; Qiu, F.; Zaia, E. W.; Wang, Z.; Kunz, M.; Guo, J.; Brady, M.; Mi, B.; Urban, J. J. Dual-Channel, Molecular-Sieving Core/Shell ZIF@MOF Architectures as Engineered Fillers in Hybrid Membranes for Highly Selective CO_2 Separation. *Nano Lett.* **2017**, *17* (11), 6752−6758.
(122) Guo, C.; Guo, J.; Zhang, Y.; Wang, D.; Zhang, L.; Guo, Y.; Ma, W.; Wang, J. Synthesis of core−shell ZIF-67@Co-MOF-74 catalyst with controllable shell thickness and enhanced photocatalytic activity for visible light-driven water oxidation. *CrystEngComm* **2018**, *20* (47), 7659−7665.
(123) Ji, M.; Lan, X.; Han, Z.; Hao, C.; Qiu, J. Luminescent Properties of Metal−Organic Framework MOF-5: Relativistic Time-Dependent Density Functional Theory Investigations. *Inorg. Chem.* **2012**, *51* (22), 12389−12394.
(124) Wan, X.; Song, H.; Zhao, D.; Zhang, L.; Lv, Y. A Y-doped metal-organic framework-based cataluminescence gas sensor for isobutanol. *Sens. Actuators, B* **2014**, *201*, 413−419.
(125) Neupane, L. N.; Oh, E.-T.; Park, H. J.; Lee, K.-H. Selective and Sensitive Detection of Heavy Metal Ions in 100% Aqueous Solution and Cells with a Fluorescence Chemosensor Based on Peptide Using Aggregation-Induced Emission. *Anal. Chem.* **2016**, *88* (6), 3333−3340.
(126) Kim, H. N.; Ren, W. X.; Kim, J. S.; Yoon, J. Fluorescent and colorimetric sensors for detection of lead, cadmium, and mercury ions. *Chem. Soc. Rev.* **2012**, *41* (8), 3210−44.
(127) Lee, M. H.; Kim, J. S.; Sessler, J. L. Small molecule-based ratiometric fluorescence probes for cations, anions, and biomolecules. *Chem. Soc. Rev.* **2015**, *44*, 4185−4191.
(128) Wang, L.; Zheng, P.; Zhang, W.; Xu, M.; Jia, K.; Liu, X. Detection of Cu^{2+} metals by luminescent sensor based on sulfonated poly T (arylene ether nitrile)/ metal-organic frameworks. *Mater. Today Commun.* **2018**, *16*, 258−263.
(129) Zhang, D.; Xu, Y.; Liu, Q.; Xi, Z. Encapsulation of $CH_3NH_3PbBr_3$ Perovskite Quantum Dots in MOF-5 Microcrystals as a Stable Platform for Temperature and Aqueous Heavy Metal Ion Detection. *Inorg. Chem.* **2018**, *57*, 4613−4619.
(130) Li, S.; Duan, Y.; Lei, S.; Qiao, J.; Li, G.; Ye, B. A new electrochemical sensing strategy for echinacoside based on an T original nanocomposite. *Sens. Actuators, B* **2018**, *274*, 218−227.
(131) Lv, Y.; Yu, H.; Xu, P.; Xu, J.; Li, X. Metal organic framework of MOF-5 with hierarchical nanopores as micro-gravimetric sensing material for aniline detection. *Sens. Actuators, B* **2018**, *256*, 639−647.
(132) Kumar, A.; Chowdhuri, A. R.; Kumari, A.; Sahu, S. K. IRMOF-3: A fluorescent nanoscale metal organic frameworks for selective sensing of glucose and Fe (III) ions without any modification. *Mater. Sci. Eng., C* **2018**, *92*, 913−921.
(133) Wei, J. Z.; Wang, X. L.; Sun, X. J.; Hou, Y.; Zhang, X.; Yang, D. D.; Dong, H.; Zhang, F. M. Rapid and Large-Scale Synthesis of IRMOF-3 by Electrochemistry Method with Enhanced Fluorescence Detection Performance for TNP. *Inorg. Chem.* **2018**, *57* (7), 3818−3824.
(134) Bhardwaj, N.; Bhardwaj, S. K.; Mehta, J.; Nayak, M. K.; Deep, A. Bacteriophage conjugated IRMOF-3 as a novel opto-sensor for S. arlettae. *New J. Chem.* **2016**, *40* (9), 8068−8073.
(135) Wang, M.; Guo, L.; Cao, D. Metal-organic framework as luminescence turn-on sensor for selective detection of metal ions: Absorbance caused enhancement mechanism. *Sens. Actuators, B* **2018**, *256*, 839−845.
(136) Zhang, J.; Liu, J.; Zhang, Y.; Yu, F.; Wang, F.; Peng, Z.; Li, Y. Voltammetric lidocaine sensor by using a glassy carbon electrode modified with porous carbon prepared from a MOF, and with a molecularly imprinted polymer. *Microchim. Acta* **2018**, *185*, 78.
(137) Xiao, L.; Zhou, S.; Hu, G.; Xu, H.; Wang, Y.; Yuan, Q. One-step synthesis of isoreticular metal−organic framework-8 derived hierarchical porous carbon and its application in differential pulse anodic stripping voltammetric determination of Pb(ii). *RSC Adv.* **2015**, *5* (94), 77159−77167.
(138) Xiao, L.; Xu, R.; Yuan, Q.; Wang, F. Highly sensitive electrochemical sensor for chloramphenicol based on MOF derived exfoliated porous carbon. *Talanta* **2017**, *167*, 39−43.
(139) Xu, W.; Thapa, K. B.; Ju, Q.; Fang, Z.; Huang, W. Heterogeneous catalysts based on mesoporous metal−organic frameworks. *Coord. Chem. Rev.* **2018**, *373*, 199−232.

DOI: 10.1021/acs.cgd.9b00879
Cryst. Growth Des. 2019, 19, 7439−7462